Astron. Astrophys. 326, 1023–1043 (1997)

ASTRONOMY
AND
ASTROPHYSICS

The angular momentum evolution of low-mass stars

J. Bouvier[1,2], **M. Forestini** [1], **and S. Allain** [1]

[1] Laboratoire d'Astrophysique, Observatoire de Grenoble, Université Joseph Fourier, B.P. 53, F-38041 Grenoble Cedex 9, France (jbouvier@laog.obs.ujf-grenoble.fr)
[2] Canada-France-Hawaii Telescope Corporation, P.O. Box 1597, Kamuela, HI 96743, USA

Received 18 February 1997 / Accepted 23 April 1997

Abstract. We present a model for the evolution of surface rotation of stars in the mass range from 0.5 to 1.1$M_\odot$, from their first appearance in the HR diagram as T Tauri stars up to the age of the Sun. The model is based on 3 assumptions: i) nearly solid-body rotation, ii) pre-main sequence disk locking, iii) wind braking. The initial conditions and the calibration of the braking law are completely determined from observations. The model includes only 2 adjustable parameters: the distribution of disk lifetimes in the pre-main sequence and the velocity at which saturation of the angular momentum losses due to the stellar wind occurs.

We review all the observational results, including the most recent ones, that can be used to constrain the models, as well as theoretical work that puts limits onto the parameter space. We show that the currently available distributions of $v\sin i$ for PMS, ZAMS and MS stars can be reasonably well reproduced by the model assuming solid-body rotation for stars in the mass-range from 0.5 to 1.1$M_\odot$. We deduce a median lifetime of 3 Myr for circumstellar accretion disks around pre-main sequence stars. By an age of 20 Myr, only 10% of the stars are still surrounded by disks. Stars with long disk lifetimes and low initial rotational velocities account for the large fraction of slow rotators ($v\sin i \leq 20$ km s^{-1}) observed in young clusters. On the opposite, stars with short-lived disk reach the ZAMS with velocities up to 200 km s^{-1} over the whole mass range investigated here.

In agreement with other models, we find that a mass-dependent saturation velocity for the angular momentum losses is required to account for the longer spin down timescale of lower mass stars on the zero-age main sequence. We argue that this assumption provides an alternative to the hypothesis of radiative core–convective envelope decoupling, which has been used in other models. Both the rapid spin down of fast rotators on the ZAMS and its mass-dependency are accounted for in the present solid-body rotation models. In particular, we show that the model predicts a distribution of rotational periods at the age of the Hyades for 0.5–1.1$M_\odot$ stars that is in close agreement with the observations.

We conclude that the observed evolution of *moderate and fast rotators* on the early main sequence requires physical processes that lead to the redistribution of angular momentum in stellar interiors on a timescale much shorter than evolutionary timescales, such as dynamical rotational instabilities, gravity waves or MHD torques. The evolution of *slow rotators* ($v\sin i \leq 10$ km s^{-1}), however, remains uncertain due to the currently uncomplete $v\sin i$ distribution. Precise $v\sin i$ measurements for slow rotators in young clusters, rather than upper limits, are required.

Key words: stars: rotation – stars: pre-main sequence

1. Introduction

The study of the angular momentum evolution of low-mass stars has known a considerable development in the last 10 years or so. As measurements of rotation rates became available for a rapidly growing number of low-mass stars located in star forming regions, young open clusters and in the field, different classes of models have been developed in order to explain the (often unexpected) observational results (see Krishnamurthi et al. 1997 for a brief review of recent models). Ultimately, modeling the rotational evolution of solar-type stars from their birth to the age of the Sun and beyond, will hopefully provide a better understanding of several important physical processes such as angular momentum loss due to stellar winds, angular momentum transport in stellar interiors, the role of circumstellar disks in the early stellar evolution, and the properties of stellar dynamos. These processes affect the rotational evolution of low-mass stars and are essential ingredients of all models developed so far.

The model proposed here differs from most previous ones by assuming that angular momentum transport is very efficient in stellar interiors. As a result, stars behave nearly as solid-bodies as they react to change in their internal structure during the pre-main sequence and to angular momentum loss at their surface. The few simple assumptions onto which the model relies are drawn from recent theoretical work and observational results and are explicited in Sect. 2. The parameters of the models are described in Sect. 3 and their effect onto the rotational evolution of low-mass stars are illustrated in Sect. 4. We review the

Send offprint requests to: J. Bouvier

observational results that can be used to constrain the models in Sect. 5 and proceed to the confrontation between the models and the observations in Sect. 6 for stars in the mass-range 0.5–1.1$M_\odot$. In Sect. 7, we discuss the plausibility of the disk lifetimes implied by the model, compare the predictions of this model to those of alternative models proposed so far, and we argue that a good match to the observations can be reached assuming that angular momentum is efficiently transported in stellar interiors.

2. Model assumptions

The model relies on the 3 following assumptions:

(H1) *Nearly solid body rotation:* we assume that solid body rotation is an acceptable approximation to the actual rotational profile of solar-type stars for the purpose of modeling the evolution of their surface rotation rate, namely:

$$\Omega(r \leq R_\star) \simeq \Omega_{surf} = \Omega_\star$$

at any time during the evolution. By this, we do not claim that stars rotate strictly as solid bodies but merely that any departure from solid body rotation is small enough so that it can be neglected for the purpose of modeling the evolution of surface rotation. More precisely, for a given total stellar angular momentum, the surface velocity computed under (H1) is assumed to be not markedly different from what it would be if computed from the (unknown) actual rotational profile. Consider the following illustrative example. A fiducial value for the total angular momentum of a solar-mass star on the main sequence is $2\,10^{48}$ g cm^2 s^{-1}. Assuming uniform internal rotation, this leads to a surface velocity of 2 km s^{-1}. If, instead, the inner radiative core ($r \leq 0.2R_\star$) rotated 3 times faster than the surface, the same value of total angular momentum would lead to a surface velocity of 1.8 km s^{-1}. In this instance, the difference in surface velocity computed for solid-body and for differential rotation is negligeable. As a consequence of (H1), the model does not allow for strong radiative core/convective envelope decoupling which is a trademark of other classes of models (e.g., McGregorq & Brenner 1991, Keppens et al. 1995). Instead, we assume that any sharp radial velocity gradients that tend to develop during PMS evolution, as the inner radiative core grows, are quickly reduced by an efficient redistribution of angular momentum throughout the stellar interior.

Except for the Sun, neither observations nor theory tell us what is the actual state of internal rotation of solar-type stars during their evolution. Depending on which physical mechanism is thought to dominate the transport of angular momentum in the stellar interior, one may expect anything from large differential rotation (from, e.g., hydrodynamical instabilities acting on evolutionary timescales) to quasi-solid body rotation (from, e.g., dynamical timescale HD instabilities, MHD processes, transport by internal waves). Helioseismology, however, does provide insight into the rotational profile of the Sun, with quite unexpected results (Gough 1990). Latitudinal differential rotation appears to be important in the solar convective zone, while the outer part of the solar radiative core, from 0.4 to 0.7 $R_\odot$, exhibits rigid rotation. Rotation in the inner core ($r \leq 0.2R_\odot$) is not yet fully constrained by helioseismology data, and contradictory claims have been made as to whether it rotates faster or slower than the outer core (e.g., Elsworth et al. 1995, Tomczyk et al. 1995, Ulrich 1993).

The largely unforeseen results of helioseismology clearly show that observations rather than theory still drive our knowledge of angular momentum transport in stellar interiors. Since the dominant physical mechanisms for angular momentum transport have not been securely identified yet (HD or MHD processes, wave transport, etc...), it may appear premature to include them a priori in the model. Furthermore, due to uncertainties in the detailed physics of these processes, none can be modeled in a deterministic way from first principles. Instead, any such process would have to be introduced in the model in a parametrized way (see, e.g., Pinsonneault et al. 1989, Chaboyer et al. 1995), and the multiplication of adjustable parameters in the models adds considerable leverage and uncertainty to an already not-so-well constrained problem. These are the main reasons why we adopt here a more empirical approach. Namely, we bypass the detailed physics of angular momentum transport in the stellar interior by postulating the internal rotational profile. This approach minimizes the number of adjustable parameters and is to be considered as a first step to get clues to the physics of the transport of angular momentum inside stars.

Nearly solid body rotation is a physically plausible expectation, and is actually observed in the Sun's radiative core, if the transport of angular momentum is dominated by short timescale HD instabilities (e.g., Endal & Sofia 1978, Pinsonneault et al. 1989, Tassoul & Tassoul 1989), MHD processes (e.g., Charbonneau 1992, McGregor & Charbonneau 1994) or internal waves (Schatzman 1993, Zahn et al. 1996, Kumar & Quataert 1997). An additional and important reason to chose this rotational profile in our approach is that it minimizes the number of adjustable parameters of the model, which is therefore better constrained by observational data. Within the same empirical approach, other choices of rotational profiles are possible and some have been explored in alternative models, at the expense of a larger number of adjustable parameters (e.g., Keppens et al. 1995). We return to the plausibility and implications of these different choices in the discussion.

(H2) *Disk locking*. As long as the young star interacts with its circumstellar disk, it retains essentially constant angular velocity, i.e.:

$$\Omega(t \leq \tau_{disk}) \simeq \Omega_o$$

where Ω_o is the initial angular velocity and τ_{disk} is the disk lifetime.

This assumption rests upon recent theoretical work and supporting observations of the rotation rates of T Tauri stars. It has been known for long that solar-mass T Tauri stars are mild rotators with equatorial velocities mostly in the 10–30 km s^{-1} range. On the other hand, Hartmann & Stauffer (1989) pointed out that if low-mass T Tauri stars accrete angular momentum from their accretion disks at a typical mass accretion rate of $10^{-7}M_\odot$yr^{-1}, they ought to be rotating much more rapidly (100–200 km s^{-1}).

And even if they were not accreting from their disk, T Tauri stars would spin up as they contract towards the ZAMS, as conventional magnetic braking due to an expanding wind is quite inefficient during early PMS evolution (Bouvier 1991). Another, much more efficient braking mechanism is therefore needed during the PMS in order to account for slow rotation.

The most popular explanation for this paradox is that the star's strong magnetosphere shreds the inner parts of the accretion disk up to beyond the corotation radius (Bertout et al. 1988, Camenzind 1990, Königl 1991). An outward flux of angular momentum then results from the magnetic torque applied by the magnetosphere onto the outer disk, which balances the inward flux of angular momentum carried onto the star by the accreted material. Although the physics of the magnetic interaction between the star and the disk is not fully elucidated yet (see, e.g. Bardou & Heyvaerts 1996), numerical simulations suggest that it quickly leads to an equilibrium where the central star evolves at roughly constant angular velocity on convective tracks (Cameron & Campbell 1993, Armitage & Clarke 1996), for values of surface magnetic fields (a few hundred gauss) and mass-accretion rates (10^{-7}-10^{-9}M$_\odot$yr^{-1}) thought to be typical of T Tauri stars (Bertout 1989). Shu et al. (1994) and Paatz & Camenzind (1996) have proposed models of the star/disk magnetospheric interaction in which a strongly collimated MHD wind results which carries angular momentum away (see Pearson & King 1995, and Popham 1996, for alternative models). Phenomenological evidence for such accretion-powered winds in young stars had been previously reported by Cabrit et al. (1990). Alternatively, Tout & Pringle (1992) suggested that energetic, dynamo-driven stellar winds from accreting T Tauri stars would lead to their rapid braking. Their model requires mass-losses of the order of 10^{-7}M$_\odot$yr^{-1}, consistent with mass-loss estimates for classical T Tauri stars. However, such dense winds disappear long before the stars reach the ZAMS and would therefore be unable to account for the slow rotators in young clusters.

The above assumption of constant angular velociy for stars interacting with their disk is supported by Cameron & Campbell's (1993) and Armitage & Clarke's (1996) models. Though many aspects of the modeling of the magnetospheric star/disk interaction remain uncertain, observations do provide independent evidence for the existence of a rotational equilibrium in accreting T Tauri stars. Measurements of the rotational periods of accreting T Tauri stars (classical T Tauri stars, CTTS) and of non-accreting T Tauri stars (weak-line T Tauri stars, WTTS) show that the former tend to rotate more slowly than the latter, the difference in the average rotation rate amounting to a factor of 2 (Bouvier et al. 1993, Edwards et al. 1993a, Choi & Herbst 1996). This result is readily interpreted in the framework of the magnetospheric disk/star coupling paradigm: accreting stars locked to their disk are prevented from spinning up as they contract and therefore remain in slow rotation, while non-accreting T Tauri stars freely spin up as their moment of inertia decreases. Not only the difference in average rotation rate, but also the very shape of the distributions of rotational periods of CTTS and WTTS is suggestive of the existence of a rotational equilibrium in CTTS. The distribution of rotational periods of CTTS is narrow and strongly peaked towards P=8d (see Fig. 2), while that of WTTS is much wider with no clear characteristic period (see, e.g, Strom 1994, Fig. 5). The strongly peaked distribution of rotational periods for CTTS by itself suggests an *equilibrium* period of the order of 8 days with a small dispersion that may reflect slightly different accretion rates and surface magnetic fields from star to star (Armitage & Clarke 1996).

On the basis of the observational evidence and theoretical modeling summarized above, the model assumes that as long as a star is surrounded by a circumstellar accretion disk, its angular velocity remains constant ("disk-locking"). Since the moment of inertia of the star strongly decreases during that phase of evolution, this implies that the central star experiences large angular momentum losses (dJ/dt=Ω_o dI/dt). The disk locking process stops as soon as the star/disk interaction ceases, and the surface angular velocity then starts to respond to structural changes in the stellar interior (as well as to conventional braking from a magnetized wind). The duration of the star/disk interaction in young stars, τ_{disk}, is an adjustable parameter of the model.

(H3) *Wind braking*. Angular momentum is extracted from the surface of low-mass stars by a magnetized stellar wind. The stellar wind acts to brake the star as soon as it decouples from its circumstellar disk in the pre-main sequence (H2) and remains instrumental for the whole subsequent evolution. The wind braking mechanism is well-funded theoretically (Schatzman 1962) and observational evidence for the magnetic braking of late-type stars on the main sequence is plentyful (e.g. Kraft 1970, Skumanich 1972, Soderblom 1983).

In order to describe this process quantitatively, the model includes a braking law which relates the angular momentum loss rate to the evolving stellar and wind properties. Activity-rotation relationships found for late-type dwarfs characterize the amplitude of magnetic activity as a function of rotation rate (e.g. Pallavicini et al. 1981, Noyes et al. 1984), and have later been shown to apply as well to pre-main sequence stars (Bouvier 1990) and subgiants (Basri 1987). Here, we adopt the formulation proposed by Kawaler (1988) which rests upon the following assumptions: i) the wind velocity at the Alfvén radius is of the order of the escape velocity, ii) the surface magnetic flux obeys a dynamo relationship of the form $R_\star^2 B \propto \Omega^a$, iii) the field geometry is parametrized by scaling the angular momentum loss rate to $(r_a/R_\star)^n$, where r_a is the Alfvén radius, with extreme values of n=2 for a radial field and n=3/7 for a dipolar field. The expression then derived for the angular momentum loss rate is:

$$\left(\frac{dJ}{dt}\right)_w = -K\ \Omega^{1+\frac{4an}{3}} \left(\frac{\dot{M}}{\dot{M}_\odot}\right)^{1-\frac{2n}{3}} \left(\frac{R}{R_\odot}\right)^{2-n} \left(\frac{M}{M_\odot}\right)^{-\frac{n}{3}}$$

where K is a calibration constant.

We follow Kawaler in assuming n=1.5, which corresponds to a field geometry "intermediate" (in some sense) between a dipolar and a radial field. In order to recover Skumanich's (1972) relationship, $\Omega(t) \propto t^{-1/2}$, which provides a reasonable approximation to the observed braking of slow rotators on the main sequence (Soderblom 1983), one must have $d\Omega/dt \propto \Omega^3$ (e.g.,

Charbonneau et al. 1995), which is obtained with a=1 in the dynamo relationship, i.e., $R_\star^2 B \propto \Omega$. Support to such a linear dynamo is provided by direct magnetic field measurements of solar-type stars that show that the integrated surface magnetic field increases with Ω up to $\Omega \simeq 10\Omega_\odot$ (Saar 1996).

For larger rotation rates, however, the dynamo relationship seems to saturate, i.e., the average surface magnetic field does not increase any more with rotation (Saar 1996). Phenomenological evidence for saturation is also provided by the study of dynamo-driven magnetic activity in late-type stars. Diagnostics of magnetic activity, i.e., coronal X-ray flux (e.g. Stauffer et al. 1994), chromospheric CaII emission (Vilhu 1984), and the size of photospheric starspots (O'Dell et al. 1995), all saturate at high rotation rates, though the angular velocity at which saturation occurs is not the same for the various activity diagnostics. The physical meaning of saturation is still unclear. It could result for instance from a saturation of the dynamo process itself due to, e.g., dynamical feedback effects of the magnetic field onto convective motions, or may reflect a saturation in the spatial coverage of the stellar surface by active regions, or other processes.

The main concern for the purpose of modeling the angular momentum evolution of low-mass stars is whether such a saturation in magnetic activity implies a corresponding saturation in the angular momentum loss rate. One cannot exclude for instance that the saturation of the activity diagnostics at high rotation rates result from the onset of other modes of radiative losses (Doyle 1996, Houdebine et al. 1996), or changing wind properties and/or magnetic field geometry. Then, one might observe a plateau in the intensity of the activity diagnostics at high rotation rates that would not necessarily imply saturated angular momentum losses. However, Barnes & Sofia (1996), following an earlier suggestion by Stauffer & Hartmann (1987), argued that saturation of the angular momentum loss rate at high velocity is required to account for fast rotators on the ZAMS. We have tried several alternative braking laws in our model (see, e.g., Mayor & Mermilliod 1990, Schatzman 1990, Charbonneau 1992) and we concur with Barnes & Sofia (1996) that, at high Ω, angular momentum losses cannot continue to increase as fast as they do at low Ω. We therefore adopt a=0 at high rotation rates in the dynamo relationship above in order to account for this saturation effect.

The angular mometum loss rate in the model is then described by the following equations:

$$\left(\frac{dJ}{dt}\right)_w = -K\,\Omega^3 \left(\frac{R}{R_\odot}\right)^{1/2} \left(\frac{M}{M_\odot}\right)^{-1/2} \qquad (\Omega < \omega_{sat})$$

and

$$\left(\frac{dJ}{dt}\right)_w = -K\,\Omega\,\omega_{sat}^2 \left(\frac{R}{R_\odot}\right)^{1/2} \left(\frac{M}{M_\odot}\right)^{-1/2} \qquad (\Omega \geq \omega_{sat})$$

where ω_{sat} is the angular velocity at which saturation occur, an adjustable parameter of the model. We return to the calibration of the braking law in the next section.

With the 3 assumptions above, the evolution of the surface velocity of low-mass stars is then fully described by the following set of equations:

$$\Omega(t) = \Omega_o \qquad (t \leq \tau_{disk})$$

and

$$\frac{1}{\Omega}\frac{d\Omega}{dt} = \frac{1}{J}\left(\frac{dJ}{dt}\right)_w - \frac{1}{I}\frac{dI}{dt} \qquad (t > \tau_{disk})$$

where $J = I\Omega$ and $I = k^2 M R^2$ is the stellar moment of inertia. During PMS evolution, after the star has decoupled from its disk, the first term on the right hand side of Eq. 2 acts to brake the star while the second term tends to spin it up as the moment of inertia decreases ($dI/dt < 0$). The evolution of surface rotation (braking or spin up) thus depends upon the relative strength of these 2 processes. We show below that the braking timescale is much longer than the evolutionary timescale during most of the PMS evolution so that PMS stars strongly spin up as they contract toward the main sequence. Once settled on the main sequence, the spin up term vanishes ($dI/dt \simeq 0$), and the star is braked by the stellar wind.

3. Model parameters

The model has only two adjustable parameters: the distribution of disk lifetimes (H2) and the angular velocity at which the angular momentum losses saturate (H3). In addition, however, one has to define realistic initial conditions for the rotation rates of solar-type stars at the beginning of their pre-main sequence evolution, to calibrate the braking-law and verify that it satisfies various theoretical and observational constraints, and use a stellar evolutionary code to follow the changes occurring in the star's internal structure during its PMS evolution. All these aspects of the model are discussed below.

3.1. Physics of the stellar evolution models

We use the stellar evolution code from Forestini (1994) in order to follow the evolution of the stellar moment of inertia, stellar radius, and radius of gyration (Rucínski 1988) as a function of time between the stellar birthline and the age of the Sun (Fig. 1). These quantities are then injected into the above set of equations to derive the evolution of surface rotation. We have modeled the rotational evolution of stars with a mass of 1.0, 0.8, and $0.5 M_\odot$. The evolutionary code does not consider the effect of mass-loss, accretion and rotation onto the stellar structure, though accretion in particular could be important during the PMS phase (Siess et al. 1997). We briefly summarize the evolutionary code below (see Forestini 1994 for a complete description).

The code solves the five one-dimensional hydrodynamical equations for the evolution of the stellar structure with the mass coordinate as independent variable. The difference equations resulting from the Henyey's procedure are solved by the Newton-Raphson relaxation method. Typically 500 (600) shells are required to model the whole pre-main sequence (main sequence) phase with 150 (200) time steps. The initial models are obtained

by solving the Lane-Emden equation with a polytropic index n = 1.5. The initial radius of these polytropic models has been chosen large enough in order to get central temperatures below $5\,10^5$ K. The initially homogeneous stars have a hydrogen mass fraction X = 0.687 for Z = 0.02, the relative heavy element abundances coming from Anders & Grevesse (1989).

The equation of state is analytic. It includes the ionization of H, He, C, N and O and the electrostatic corrections through the statistical model of Debye-Hückel for partially ionized regions and through the interpolation formalism of Koester (1976) for completely ionized matter. Generalized Fermi-Dirac integrals have been very accurately computed for the treatment of electronic degeneracy.

At low temperatures, i.e. below 8000 K, we use the Alexander & Ferguson (1994) opacity tables, very well suited for cool red giant envelopes and atmospheres. At temperatures above 8000 K, we use the OPAL opacity tables computed by Rogers & Iglesias (1992). Finally, we used the Hubbard & Lampe (1969) program to generate conductive opacity tables corresponding to the same chemical compositions as for the OPAL radiative opacity tables.

The stellar structure is integrated from the center to a very low optical depth (τ = 0.001) in the atmosphere. For optical depths $\tau < 10$, the temperature profile and derivative quantities (such as the radiative pressure and gradient) are constrained by atmosphere models of Plez (1992) for $T_{\rm eff} < 3900$ K, of Eriksson (1994, private communication) up to 5500 K; above this effective temperature, atmosphere models are generated with the Kurucz atmosphere program.

The structure of the convective regions is computed using the classical Mixing-Length Theory (MLT), as prescribed by Kippenhahn et al. (1968). Our models are standard in the sense that the Schwarzschild criterion is considered to delimit the convective zones and neither overshooting nor semi-convection have been considered in the present computations. The ratio α of the mixing-length free parameter over the pressure scale height has been put to a value of 1.5, i.e. rather close to $\alpha_\odot$ = 1.64 with which we fit the solar structure.

The nucleosynthesis equations are solved using the Wagoner (1969) numerical technique. The abundance evolution of all the stable and unstable nucleides involved in proton burning are followed through a nuclear reaction network for which the nuclear reaction rates are taken from Caughlan & Fowler (1988). The nuclear screening factors are parameterized by using the Graboske et al. (1973) formalism, including weak, intermediate and strong screening cases.

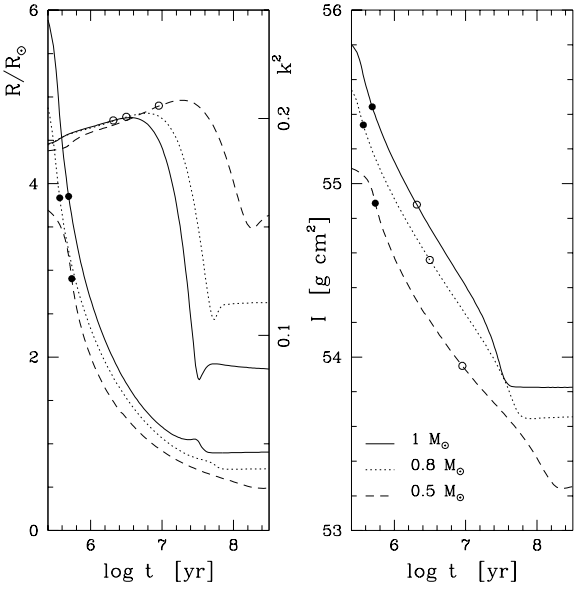

Fig. 1. Evolution of the stellar radius, radius of gyration and moment of inertia of 0.5, 0.8 and 1M$_\odot$ stars. Black dots indicate the time at which the star appears on the stellar birthline (for a mass-accretion rate of 10^{-5}M$_\odot$yr^{-1}, Hartmann et al. 1997), and empty dots show the time at which the radiative core starts to develop.

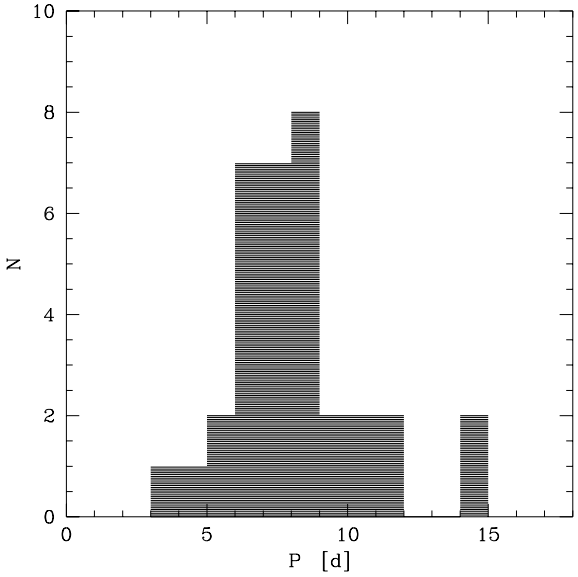

Fig. 2. Histogram of rotational periods of low-mass classical T Tauri stars.

3.2. Initial conditions

Solar-type stars retain the memory of their initial angular momentum up to an age of a few 10^8 years (and up to almost 1 Gyr for the very low mass stars). It is therefore of prime importance that the initial conditions injected into the model bear some ressemblance with the rotation rates actually observed for the youngest stars. We argue here that the distribution of the rotational periods of accreting T Tauri stars (CTTS) provides the proper initial conditions.

Fig. 2 shows the distribution of P_{rot} of CTTS (Bouvier et al. 1993, 1995 and references therein, Edwards et al. 1993a). The distribution strongly peaks at a characteristic rotational period of 7–9 days. We argued in the previous section that the shape of the distribution supports the view that accreting T Tauri stars have reached a rotational equilibrium under which their angular velocity does not change with time. In other words, this "equi-

librium" distribution is invariant in time as long as the stars continue to accrete from their disk. Thus, even though the stars plotted in Fig. 2 have ages between about 1 and 4 Myr, the same distribution of P_{rot} applies to stars on the birthline, i.e., at an age of a few 0.1 Myr. An implicit assumption here is that all solar-type stars are born with disks. If this were not the case, some stars might have already spun up as they appear on the birthline and some rapid rotators would have to be included in the initial conditions. This is not supported by the observations: all low-mass stars close to the birthline have rotation rates far below break-up (Bertout 1989, Fig. 4) and the ubiquity of strong IR excesses exhibited by the youngest stars in deeply embedded clusters support the view that all stars are born with accretion disks (Strom 1995). Measurements of the rotational velocity of the youngest, still deeply embedded, stars also indicate low rotation rates (Casali & Eiroa 1996).

For pratical purpose, we approximate the observed distribution of rotational periods by an analytical function. We find that the observed distribution is very well fitted by a Gaussian curve with a mean period of 7.8d and a dispersion of 2.0d (KS test probability of 0.96). Hence, the frequency distribution of initial periods is given by:

$$f_{P_o}(P_o) = \frac{1}{2\sqrt{2\pi}} \cdot \exp\left[-\left(\frac{P_o - 7.8}{2\sqrt{2}}\right)^2\right]$$

from which the distribution of initial angular velocities, $\Omega_o = 2\pi/P_o$, is obtained. Because the rotation rates of low-mass T Tauri stars do not seem to strongly vary with mass below $1M_\odot$ (Bouvier 1991), we adopt the same initial conditions for modeling 0.5, 0.8 and $1.0M_\odot$ stars. We emphasize again that the star retains the Ω_o it had on the birthline until it uncouples from its disk (H2). Therefore, the Ω_o thus derived also corresponds to the velocity the star has at $t = \tau_{disk}$. And since τ_{disk} varies from star to star, this explains how the large angular momentum spread observed on the ZAMS builds up during PMS evolution (Bouvier et al. 1993, Edwards et al. 1993a).

Based on a larger sample, Choi & Herbst (1996) found that the distribution of rotational periods of PMS stars in Orion is bimodal, with a slow rotator group centered at $P_{slow} = 8.3d$ and a fast rotator group at $P_{fast} = 2.55d$. They interpret the slow rotators as being locked to their disk while fast rotators correspond to non-accreting stars. The mean period (8.3d) and the dispersion (3.8d) of the slow rotator group are in rough agreement with the numbers derived from the sample discussed above (part of the larger dispersion derived by Choi & Herbst comes from the detection of a 34.5d period which was later dismissed –Herbst, priv. comm.–). We ran test models using Choi & Herbst's mean and dispersion values for the distribution of initial periods and found no significant difference in the results.

3.3. Angular momentum loss

The saturated braking law described above is calibrated by requiring that $1M_\odot$ stars reach the age of the Sun with the solar angular velocity, i.e.:

$$\Omega(t = t_\odot) = \Omega_\odot = 2.9\ 10^{-6} s^{-1}$$

which yields K=2.7 10^{47} in the expression of the braking-law above. We emphasize that this calibration does not depend upon initial velocities nor upon the distribution of disk lifetimes. This is because, by the time the stars have reached the age of the Sun, all have converged to the same surface velocity regardless of their past rotational history (see Fig. 4). The calibration is therefore uniquely determined by the Sun.

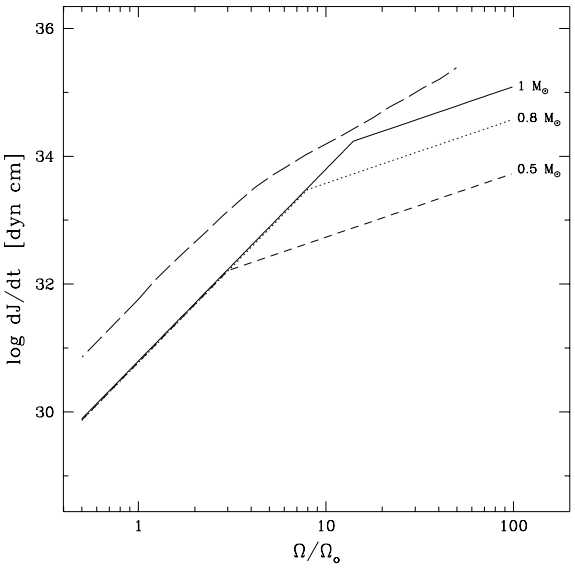

Fig. 3. Angular momentum loss rate as a fuction of angular velocity for 0.5, 0.8 and 1.0 $M_\odot$ stars. The angular momentum loss rates saturate at $\Omega = 3, 8, 14\Omega_\odot$ for 0.5, 0.8, and 1.0 $M_\odot$ stars, respectively. The dashed line is the J loss rate *upper limit* computed by Charbonneau (1992) on the basis of the Weber-Davis solar-wind model.

Thus completely defined, the braking-law still has to meet two constaints. First, it must predict the "observed" angular momentum loss rate of the Sun, whose reported value varies between 3 10^{30} dyn cm (Pizzo et al. 1983) and 6 10^{30} dyn cm (Mihalas 1973). Evidently some uncertainty remains about the exact value of $\dot{J}_\odot$ because it scales as the square of the Alfvén radius, which is still poorly known for the Sun (e.g., r_a = 12 $R_\odot$ in Pizzo et al., 37 $R_\odot$ in Keppens et al. 1995), and also because it depends on the elusive (and varying) 3D geometry of the Sun's magnetic field. Nevertheless, the calibrated braking law predicts $\dot{J}(t = t_\odot) = 6.6\ 10^{30}$ dyn cm, which is consistent with the $\dot{J}_\odot$ estimate. Second, Charbonneau (1992) has derived an *upper limit* to the angular momentum loss rate that solar-mass stars experience on the main sequence. Using the 2D Weber & Davis (1967) equatorial solar-wind model, and assuming a linear dynamo relationship ($R_\star^2 B \propto \Omega$), he computed $\dot{J}(\Omega)$. Because of the assumed purely radial field geometry, which maximizes the J losses (see, e.g., Mestel 1984), any braking law relevant to more realistic 3D magnetic field geometries in late-type stars must predict lower J losses than Charbonneau's

one at all Ω's (although there probably remains enough uncertainty both in the dynamo process and in the wind properties of low-mass stars that one cannot completely exclude that $\dot{J}$ does not exactly behaves as predicted from an extrapolation of the Weber-Davis model to fast rotators). Fig. 3 shows that the braking law adopted here indeed predicts lower J loss rates than Charbonneau's, as can be expected from the more complex field geometries that prevail at the surface of low-mass stars, and the asymptotic behaviour of the two braking laws at low velocities is the same ($\dot{J} \propto \Omega^3$).

The change in the slope of the braking law beyond $\omega_{sat} = 14\Omega_\odot$ (for 1 $M_\odot$ models) illustrates the saturation of angular momentum loss rates at high velocities (H3). The "best-fit model" discussed below assumes that $\dot{J}$ scales as Ω in the satured regime (instead of Ω^3 in the unsaturated regime). It should be emphasized, however, that this parametrized description of the saturation of the angular momentum losses may not be unique. We certainly lack the clear physical understanding of the saturation process which would allow us to predict the exact form of the saturated law. As an example, Bouvier & Forestini's (1994) model included a saturated J loss law where $\dot{J}$ scaled as Ω^2 (as in Mayor & Mermilliod 1990), and still produced very fast rotators at the ZAMS.

3.4. Disk lifetimes

By disk "lifetime" we more precisely mean the duration of the disk-coupling process which locks the star at a constant angular velocity (H2). The disk lifetime, τ_{disk}, thus refers to disks which sustain a large enough mass-accretion rate so that the rotational equilibrium does not break down (Cameron & Campbell 1993, Armitage & Clarke 1996). The distribution of τ_{disk} is a central parameter of the model since it is primarily the duration of the disk-locking process during PMS evolution that dictates the angular velocity of the star at the ZAMS. Short-lived disk will let the star spin up during most of its PMS evolution, and thus produce fast rotators on the ZAMS, while long-lived disk will prevent the PMS spin up, and thus lead to slow rotators on the ZAMS. We consider the distribution of disk lifetimes as an adjustable parameter of the model, thus hoping to get insight into the duration of the accretion phase during PMS evolution from a completely new perspective. Nevertheless, observational studies of PMS stars help to put constraints on plausible disk lifetime distributions.

Observational estimates of the frequency of circumstellar disks around young stars are conventionally obtained from the statistics of disk diagnostics among PMS stars. Among the various available diagnostics, the study of near-IR excess and mm emission have provided the best estimates of disk frequency so far. Near-IR excess correlates with other accretion diagnostics (e.g., veiling, UV excess, broad H_α emission, see Hartigan et al. 1990, Edwards et al. 1993b) as does mm emission (André & Montmerle 1994, Osterloh & Beckwith 1995) and are indicative of optically *thick* disks, i.e., disks which sustain accretion rates larger than a few $10^{-9} M_\odot yr^{-1}$. At lower accretion rates, the disk becomes optically thin, and accretion diagnostics (veiling, broad Balmer emission, forbidden lines) fade to marginally detectable levels (see Strom et al. 1993). Only a mild IR excess may be expected to persist for some time in partially optically thin disks due to reprocessed stellar light, though Hartigan et al. (1995) found that the near-IR excess disappears altogether when other accretion diagnostics do.

The main results of surveys of IR excess and mm emission among large samples of PMS stars can be summarized as follow: i) the survival time of optically thick disks varies from star to star between a few 0.1 Myr and 10 Myr or more (Walter et al. 1988, K.M. Strom et al. 1989); ii) the frequency of optically thick disk evolves with time from 60–100% in the youngest observable objects in deeply embedded clusters (Strom 1995, Lada et al. 1996, Greene & Meyer 1995), to 30–50% at an age of 3–5 Myr (Strom et al. 1989, Skrutskie et al. 1990, Lada et al. 1993, K.M. Strom et al. 1993, Hughes et al. 1994, Kenyon & Hartmann 1995), and down to 10–30% at 10 Myr (e.g. Strom 1995, Lawson et al. 1996); by an age of 50–100 Myr, no optically thick disk remains (Skrutskie et al. 1991, Zuckerman & Becklin 1993, Trullols & Jordi 1993); iii) the transition between optically thick and optically thin disks occurs very rapidly on a timescale of a few 0.1 Myr (Strom et al. 1989, André & Montmerle 1994, Osterloh & Beckwith 1995).

These disk frequency estimates are based on surveys of PMS stars with ages usually less than 10 Myr and located in the central, densest parts of molecular clouds. More recently, however, ROSAT X-ray surveys of star forming regions have led to the discovery of tens of new PMS stars scattered over much larger areas, none of which seems to exhibit significant IR excesses (e.g. Alcalá et al. 1996, Wichmann et al. 1996). Adding these new WTTS into the statistics of IR excesses above would reduce the overall disk frequency (Feigelson et al. 1993, Neuhaüser et al. 1995). It has been suggested that at least part of this widespread ROSAT population may consist of WTTS significantly older than those previously known (Sterzik & Durisen 1995, Feigelson 1996 and references therein, see also Walter et al. 1988) and age measurements for a few of these stars, obtained from isochrone fitting in the HR diagram, seems to support their post-TTS status with an age larger than 10 Myr (Alcalá et al. 1997, Wichmann et al. 1997a, see however Briceño et al. 1997 for another view). The existence of a large population of such diskless, evolved T Tauri stars, would indeed confirm the rapidly decreasing disk frequency among aging PMS stars.

These results provide a basis for defining the distribution of τ_{disk}. In the model discussed below, we assumed the simplest form for this distribution which is consistent with the observations, namely: all stars on the birthline are coupled to their disk (as suggested by the ubiquity of IR excesses among embedded cluster members), and the disk frequency decreases as 1/t thereafter. The frequency distribution of disk lifetime is then given by:

$$f_{\tau_{disk}}(\tau_{disk}) = \frac{1}{(\ln t_f - \ln t_{bl})} \cdot \frac{1}{\tau_{disk}} \cdot g(\tau_{disk})$$

where t_{bl} is the time at which the star appears on the birthline (Stahler 1988, Hartmann et al. 1997) and t_f is the maximum

disk lifetime, set to 40 Myr here (all stars are coupled to their disk at t_{bl}, and none at t_f). The term $g(t)$ is an apodizing function which ensures that $f_{\tau_{disk}}(t_f) = 0$.

The integration of this distribution over time yields the fraction of stars which remain coupled to their disk up to a given age:

$$\frac{N_{disk}}{N_{tot}}(t) = 1 - \int_{t_{bl}}^{t} f_{\tau_{disk}}(\tau_{disk}) d\tau_{disk} \leq 1 - \frac{\log t - \log t_{bl}}{\log t_f - \log t_{bl}}$$

where the $\leq$ sign arises from the apodizing function included in $f_{\tau_{disk}}(t)$. For $0.8 M_\odot$ models ($\log t_{bl} \simeq 5.5$), the fraction $N_{disk}/N_{tot}(t)$ amounts to 100% at 0.3 Myr, 50% at 3 Myr, 20% at 10 Myr, and 10% at 20 Myr. No disk remains beyond 40 Myr. These numbers are consistent with the upper bounds of the estimates of disk frequency among PMS stars drawn from IR excess surveys.

We emphasize again that $N_{disk}/N_{tot}(t)$ represents the fraction of stars surrounded by disks *that sustain mass-accretion at a large enough rate as to lock the central star at constant angular velocity* (H2). According to Cameron & Campbell (1993), once the rotational equilibrium is reached early in the star's evolution, it remains instrumental until the mass-accretion has dwindled to values as low as a few $10^{-11} M_\odot \mathrm{yr}^{-1}$. At such a low accretion rate, the disk is completely optically thin and the system may have spectral properties similar to those of WTTS (Strom et al. 1993, Hartigan et al. 1995). In other words, the disk frequency estimates based on the statistics of near-IR excesses merely provides a lower limit to the fraction of stars that may actually be coupled to their (optically thin) disk (Armitage & Clarke 1996). We return to the plausibility of long-lived disks in the discussion.

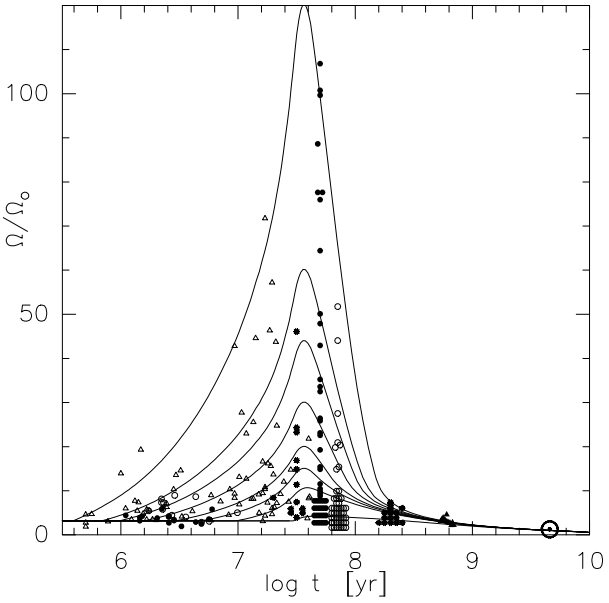

Fig. 4. Grid of rotational tracks for 1 $M_\odot$ stars (P_o = 8d, $\omega_{sat} = 14\Omega_\odot$). The upper track depicts the evolution of surface rotation for stars with short disk lifetimes (τ_{disk} = 0.4 Myr) and the lower one for stars with long-lived disks (τ_{disk} = 30 Myr). Note how sensitive is the peak velocity on the ZAMS to the disk lifetime. For reference, observed angular velocities (computed from periods or projected linear velocities) are shown for low-mass T Tauri stars ($\leq$1–5 Myr), post-T Tauri stars (5–20 Myr), and G-type members of the IC 2602 (30 Myr), IC 2391 (30 Myr), Alpha Persei (50 Myr), Pleiades (80 Myr), M34 (225 Myr), M7 (225 Myr) and Hyades clusters (600 Myr), and the Sun (see Appendix). The groups of stars in young clusters shown at $\Omega/\Omega_\odot \leq 5$ have $v\sin i$ upper limits of 7 to 10 km s^{-1}.

4. Effect of the parameters

The angular momentum evolution of a given star depends upon its initial angular momentum (Ω_o), the lifetime of its disk (τ_{disk}) and the wind braking it experiences (ω_{sat}). We describe here how each of these parameters affect the rotational evolution.

Fig. 4 shows a grid of rotational tracks, $\Omega(t)$, for the $1 M_\odot$ model. The grid is computed for an initial velocity $\Omega = 3\Omega_\odot$, which corresponds to an initial period of 8d, and for several disk lifetimes ranging from 0.4 Myr to 30 Myr. The observational data superimposed on the tracks for reference are discussed in the next section. This figure clearly illustrates how the stellar velocity on the ZAMS is related to the disk lifetime. Angular velocities up to $100\Omega_\odot$ and more are reached by the age of young clusters when the disk dissipates very early in the star's PMS evolution ($\tau_{disk} \leq 1$ Myr) while velocities of the order of $5\Omega_\odot$ result from the longest τ_{disk} (≥ 10 Myr). Hence, to a large extent, τ_{disk} dictates the angular velocity the star has as it settles on the ZAMS. The velocity at ZAMS also depends, albeit to a lower extent, upon the initial velocity. This is shown in Fig. 5 where rotational tracks are shown for 3 initial velocities which span most of the range allowed by the distribution of initial periods. For short τ_{disk}, stars with high initial angular momentum reach the ZAMS as ultrafast rotators while those with initally low angular momentum are more moderate rotators on the ZAMS. For long τ_{disk}, stars with low initial angular momentum reach the ZAMS as ultraslow rotators.

The evolution of rotation during PMS contraction is hardly affected by wind braking. The reason is that the wind braking timescale is much longer than the contraction timescale for most of the PMS evolution. This is shown in Fig. 6 where various relevant timescales are compared. The contraction timescale is orders of magnitude shorter than the braking timescale up to an age of about 20 Myr. Hence, wind braking cannot prevent the star to spin up as it contracts towards the ZAMS. As the star approaches the ZAMS, however, the contraction timescale rapidly lengthens and eventually, at an age of about 30 Myr, becomes comparable to the braking timescale for fast rotators. As a result, stars begin to spin down as soon as they settle on the ZAMS (and, in fact, slightly earlier). For fast rotators ($\Omega \simeq 100\Omega_\odot$), the braking timescale is then quite short ($\simeq 50$ Myr), and they are quickly spun down on the ZAMS. For slow rotators ($\Omega \simeq 5\Omega_\odot$), however, the braking timescale is of the order of 1 Gyr, and they spin down at a much slower pace on the main sequence.

It is precisely because wind braking is ineffective during PMS evolution that disk braking, through the magnetic star-disk interaction, has to be called upon to understand how some

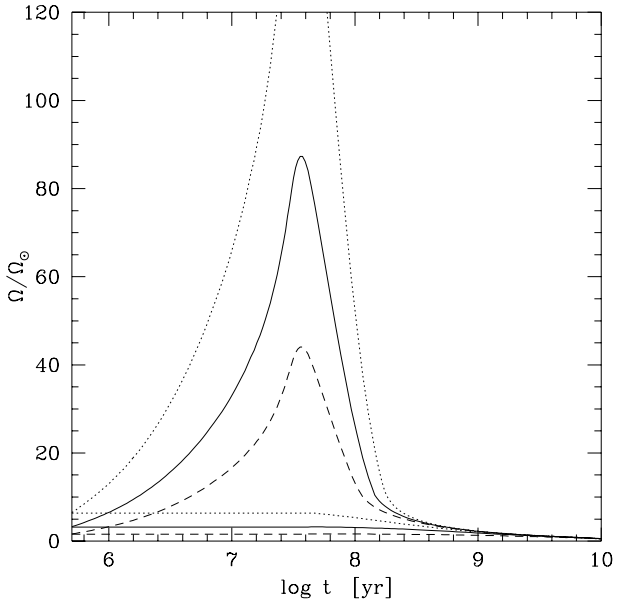

Fig. 5. Rotational tracks (ω_{sat} = 14$\Omega_\odot$) for 1 $M_\odot$ stars with initial periods of 4, 8, and 16 days, respectively. For each initial period, two tracks are shown corresponding to short- and long-lived disks respectively. Since the initial periods shown in this figure encompass most of the range allowed by the gaussian period distribution used in the model, the upper track (shortest initial period, short-lived disk) illustrates the upper envelope of the rotational evolution of 1 $M_\odot$ stars, and the lower track (longest initial period, long-lived disk) the lower envelope.

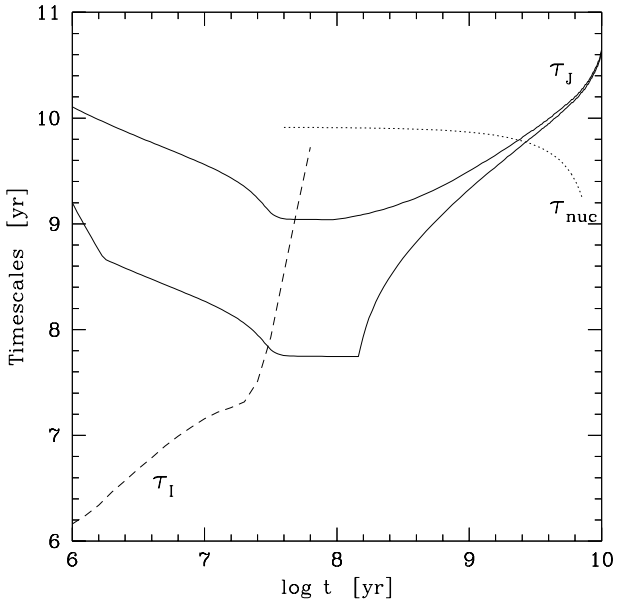

Fig. 6. Timescales for PMS contraction τ_I, wind braking τ_J, and nuclear evolution on the main sequence τ_{nuc} (1$M_\odot$ stars). The braking timescale (1/J dJ/dt)$^{-1}$ is shown for slow rotators (τ_{disk} = 30 Myr, upper solid curve) and fast ones (τ_{disk} = 0.4 Myr, lower solid curve), whose rotational tracks are plotted in Fig. 4 (lower and upper tracks, respectively). The contraction timescale (1/I dI/dt)$^{-1}$ (dashed curve) remains very short compared to the braking timescale for most of the PMS evolution, so that braking cannot prevent the stars from spinning up as they contract toward the ZAMS. Over the first few Gyr on the main sequence, the braking timescale is shorter than both the contraction and nuclear timescales (1/[H] d[H]/dt)$^{-1}$), and stars are then efficiently braked.

PMS stars are prevented to spin up on their convective tracks. As long as the star-disk coupling is instrumental, the star maintains roughly constant angular velocity. Then, the disk braking timescale is equal to the contraction timescale. It is seen from Fig. 6 that the disk braking timescale is much shorter than the wind braking timescale during all the PMS evolution. We therefore neglected wind braking whenever disk braking is active, i.e., as long as the stars are coupled to their disk.

The spin-down timescale of fast rotators on the ZAMS is very sensitive to the value of the velocity at which dynamo saturation occurs, ω_{sat}. The reason is twofold and is illustrated in Fig. 7 where rotational tracks are shown for ω_{sat} of 10$\Omega_\odot$ and 14$\Omega_\odot$, respectively. Firstly, because saturated J losses are proportional to ω_{sat}^2, a lower value of ω_{sat} leads to less efficient braking. This is true during the PMS evolution, and the star will thus reach a higher peak velocity at the ZAMS, and is also true on the ZAMS, so that the star will take more time to spin down. Secondly, the lower the value of ω_{sat}, the longer the time spent into the saturated J loss regime. These 2 effects thus concur to lengthen the spin down timescale of fast rotators on the ZAMS as ω_{sat} decreases. Fig. 7 shows that all stars have converged down to low velocities by an age of 200 Myr for ω_{sat} = 14$\Omega_\odot$, while the convergence does not occur before at least 400 Myr for ω_{sat} = 10$\Omega_\odot$. Then, the value of ω_{sat} will be best constrained by the observed spin down rate on the early ZAMS (between the 50 Myr Alpha Persei and the 80 Myr Pleiades clusters) and, even more, by clusters whose age is intermediate between that of the Pleiades (80 Myr) and that of the Hyades (600 Myr). Such intermediate-age clusters will precisely indicate when the convergence of rotation rates is completed on the main sequence (e.g., M34, M7, see below).

In summary, the central parameter for the evolution of angular momentum during the PMS is the distribution of disk lifetimes, which largely dictates the velocity distribution at the ZAMS. The critical parameter for ZAMS and early MS rotational evolution is the value of ω_{sat} at which J losses saturate. However, these 2 adjustable parameters of the model are not separable. Varying one or the other impacts on both the PMS and the MS evolution of surface rotation. This is why the evolution of surface rotation has to be modeled consistently all the way from the T Tauri phase to the age of the Sun. Modeling only part of it (e.g., the PMS contraction phase, or the ZAMS spin down phase) does not account for the wealth of constraints now available from the observations of PMS, ZAMS and MS stars.

5. Observational constraints

In the previous sections, some observational constraints were already included into the model to define boundary conditions. This is the case of the distribution of rotational periods of clas-

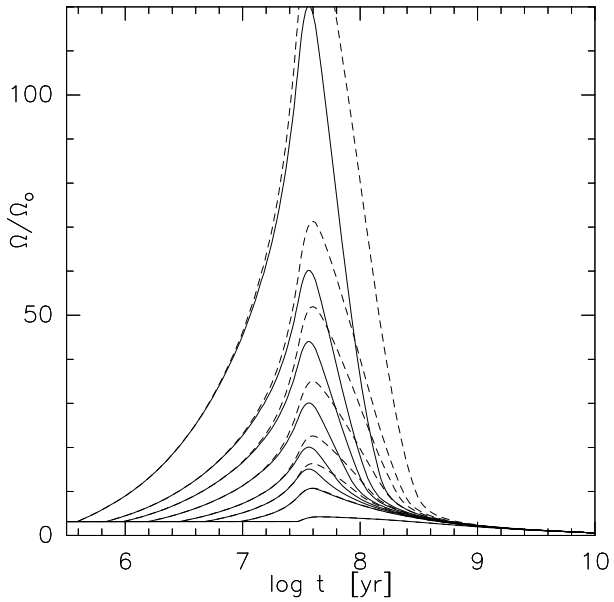

Fig. 7. Sets of rotational tracks for $1M_\odot$ stars with $\omega_{sat} = 14\Omega_\odot$ (solid curves) and $\omega_{sat} = 10\Omega_\odot$ (dashed curves). A lower value of ω_{sat} leads to higher peak velocities at the ZAMS and longer spin down timescales (see text).

sical T Tauri stars, which defines the initial angular momentum distribution, and of the Sun's surface velocity, which was used to calibrate the braking law.

Since the model aims at accounting for the observed PMS and MS evolution of surface rotation in stars with a mass between 0.5 and $1.0M_\odot$, it is constrained by measurements of rotational periods and velocities for stars in this mass range at various evolutionary phases. Rotational data are now available for PMS stars in several star forming regions, with an age between typically 1Myr and a few 10Myr, for late-type dwarfs belonging to young clusters (30–100 Myr old, e.g., IC 2391, IC 2602, Alpha Per, Pleiades), to intermediate-age clusters (200 Myr old, M7, M34), and to old clusters (600 Myr old, Hyades), and for field stars ($\geq$ 1Gyr old). Even though most rotational distributions are still incomplete (and some are drawn from small samples indeed), this wealth of data gathered in the last few years allows one to trace observationally the evolution of surface rotation of solar-type stars with a relatively good accuracy. All these constraints have to be considered simultaneously for a proper comparison between the model and the observations.

We provide in the Appendix a complete list of the samples from which the observed rotational distributions were drawn with relevant references. Among the best studied clusters are Alpha Persei, Pleiades, and Hyades. Each of these clusters has its own interest. At an age of 50 Myr ($\pm$ 10Myr), Alpha Persei includes G stars recently arrived on the ZAMS. Since the model predicts that this is precisely the time when $1M_\odot$ stars reach their peak velocity, the maximum velocities observed for G stars in this cluster will provide a strong constraint to the model. The Pleiades cluster is only slightly older than Alpha Persei with an age estimated to lie between 70 and 110 Myr. Therefore, the comparison of rotational distributions between the 2 clusters brings insight into the spin down timescale on the ZAMS for stars of different masses. Finally, the 600 Myr old Hyades cluster is the only one for which a tight relationship between rotational period and stellar mass has been demonstrated (Radick et al. 1987): by that age, all stars more massive than $0.5M_\odot$ have converged to very low velocities ($v\sin i \leq 10\,\mathrm{km\,s^{-1}}$), while the least massive stars still include fast rotators (Stauffer et al. 1997a). This cluster thus provides a very strong constraint to the convergence timescale of the rotation rates on the main sequence as a function of stellar mass. Even though other clusters have not been as extensively studied yet, some already provide important results against which the model has to be confronted. This is the case in particular of intermediate age ($\simeq$ 200 Myr old) clusters (M34, Jones et al. 1997, M7, Prosser et al. 1995). Because they fill the age gap between the Pleiades cluster (which includes many fast rotators) and the Hyades cluster (in which all stars rotate slowly), the rotation rates of the low-mass members of these clusters provide a much more accurate determination of the spin down timescale for solar-type stars on the main sequence than that previously drawn from the comparison between Pleiades and Hyades alone.

6. Model vs observations

In order to compare the model with observations, we compute synthetic distributions of rotational velocities from the model using a Monte-Carlo method. Synthetic samples of 20,000 stars were considered in order to reduce the statistical noise to negligeable levels. An initial angular velocity is assigned to each star on the birthline, following the frequency distribution of initial periods described above. Each star is also given a disk lifetime, which is randomly drawn from the distribution of τ_{disk}. The pair (Ω_o, τ_{disk}) then completely defines the rotational evolution of the star. In order to reduce computation time, we build grids of rotational tracks $\Omega(t, \Omega_o^i, \tau_{disk}^i)$ and interpolate into these grids to derive the velocity of each star at a given time. The distribution of equatorial velocity can thus be drawn for the 20,000 stars at any arbitrary time in their evolution. Because most of the observations provide distributions of projected velocities, $v\sin i$, the synthetic distributions of equatorial velocities are converted into a distribution of projected velocities by multiplying each velocity by $\sqrt{2p - p^2}$ where p is a random number between 0 and 1. The comparison between synthetic and observed distributions is then made using histograms with $10\,\mathrm{km\,s^{-1}}$-wide bins, which corresponds to the resolution limit of many $v\sin i$ studies.

The definition of proper stellar samples to be compared with model distributions of $v\sin i$ is not straightforward. On the one hand, the samples must be large enough to provide a statistically meaningful comparison. On the other, they must be restricted as much as possible to a narrow mass range around the stellar mass for which the model has been computed. In principle, we are able to compute models for stars with a mass between 0.5 and $1.1M_\odot$ by steps of $0.1M_\odot$. However, the $v\sin i$ samples available for such narrow mass ranges (e.g., 0.45–0.55$M_\odot$, 0.55–0.65$M_\odot$,

etc..) would be far to small to be compared with the models. We were therefore led to bin the observed $v\sin i$ samples over larger mass ranges. Examination of the $v\sin i$ distribution of late-type stars in young clusters helps to properly define acceptable mass ranges. For instance, in the Pleiades cluster, $1M_\odot$ stars are already spun down while $0.8M_\odot$ are not. This forbids one to include $0.8M_\odot$ stars in the $1.0M_\odot$ the stellar sample. We therefore defined a first mass range between 0.9 and $1.1M_\odot$ to be compared with $1M_\odot$ models. On the opposite, stars in the mass range between 0.6 and $0.9M_\odot$ in young clusters have very similar $v\sin i$ distributions. We therefore defined a second mass range from 0.6 to $0.9M_\odot$ to be compared with $0.8M_\odot$ models. Finally, stars with a mass less than $0.6M_\odot$ were used to define the third mass range which we compare with $0.5M_\odot$ models. The only exception to this procedure is for T Tauri stars, where all stars in the 0.5–$1.1M_\odot$ range were binned in the same sample in order to increase the sample size. This appears justified by the lack of a strong dependency of rotation upon mass within these mass limits and by the uncertainty affecting mass estimates for young PMS stars (Bouvier 1991).

We shall assume that the various samples of PMS stars, cluster stars and field stars define an age sequence. This is not necessarily true, however, since PMS stars belong to loose associations which will quickly dissipate while cluster stars formed in a much denser environment. Whether the different modes of star formation implied by associations and bound clusters (Lada et al. 1991) impact on the distribution of initial angular momenta is currently unknown. In addition, several sources of uncertainties may affect the observed $v\sin i$ distributions: i) the measurement error on $v\sin i$ is usually of the order of 10%; however, especially for slow rotators close to the detection limit (7–10 km s^{-1} for most studies), the uncertainties can be larger. Hence, the relative number of stars in the 0–10 and 10–20 km s^{-1} bins is sometimes quite uncertain; ii) the age of the clusters depends upon the method used to date them and upon the detailed physics of the evolutionary models used for isochrone fitting (e.g. convective overshooting). As an example, the Pleiades have been assigned an age of 70, 80, 100 and 110 Myr by different authors (see Appendix); iii) for some clusters (e.g. Alpha Persei, M34), membership is sometimes difficult to assess and contamination by (slow rotating) field stars may not be negligeable; iv) some samples (PTTS, IC2602, IC2391) are X-ray selected. Because there exists a tight relationship between X-ray flux and rotation, with the fastest rotators being the brightest X-ray sources, these samples are likely to be biased against slow rotators; v) not all clusters have the same metallicity and it is not known how metallicity may affect the angular momentum evolution of stars; vi) finally, at least half of the stars are probably members of binary systems. While in wide systems the $v\sin i$ distribution of single and binary stars appear similar (Bouvier et al. 1997b), the 10% or so short period spectroscopic binaries might experience quite a different rotational evolution than single stars and wider systems. Keeping these uncertainties in mind, the comparison between models and observations in the 3 mass ranges is presented in the next sections.

6.1. 1 $M_\odot$ model

The observed $v\sin i$ distributions of stars in the 0.9–$1.1M_\odot$ range are shown in Fig. 8. The synthetic distributions computed from the $1M_\odot$ models with ω_{sat}=$14\Omega_\odot$ are shown in Fig. 9 at corresponding ages. The first panel shows the $v\sin i$ distribution of T Tauri stars at 1 Myr. The agreement between the model and observations there is not very surprising: the stars started their evolution on the birthline at an age of 0.5 Myr and less than 20% of them have dissipated their disk at 1 Myr. Therefore, the predicted distribution at 1 Myr is fairly close to the initial distribution defined by CTTS rotational periods. At an age of 20 Myr, taken as being representative of the post-T Tauri star sample, a high velocity tail has developed to more than 100 km s^{-1} as stars with short-lived disk have spun up. Simultaneously, stars still coupled to their disk pile up in the lowest $v\sin i$ bins as their angular velocity remains constant and their radius decreases. Comparison between the 20 Myr distribution and that of post-TTS shows that the latter contains much less slow rotators than predicted by the model. This is very likely because the sample is X-ray selected and therefore biased against the detection of the slowest rotators (Bouvier et al. 1997a). Peak velocities are reached at 30 Myr, just before the $1M_\odot$ stars land on the ZAMS. The model predicts maximum velocities of about 170 km s^{-1} at that age. Even though the young IC clusters sample is too small to allow a detailed comparison, the predicted and observed distributions cover a similar range of rotation rates. At 50 Myr, the estimated age of the Alpha Persei cluster, the ZAMS spin down has started: the high velocity tails has slightly decreased to 150 km s^{-1}, and the fraction of slow rotators begins to increase. The model predicts 50% of the stars with $v\sin i$ less than 20 km s^{-1} at that age, while observations suggest a fraction of 60% such slow rotators. The rest of the evolution is characterized by a sharp spin down: the high velocity tail has receded down to 80 km s^{-1} at an age of 80 Myr and to 50 km s^{-1} at 100 Myr while the fraction of very slow rotators considerably increases. The model distribution at 100 Myr is in fact remarkably similar to that of the Pleiades with 80% of the stars below 20 km s^{-1} and a maximum velocity of 50 km s^{-1}, which tends to support the 100 Myr age estimate of Meynet et al. (1993). Later on the MS, at an age of 200 Myr, the model predicts that most stars rotate at less than 10 km s^{-1}. Observations suggest a slightly larger fraction of rotators in the 10–20 km s^{-1} bin than predicted by the model. Soderblom (1996) argued that the moderate rotators in M34 is evidence for differential rotation in the stellar interior: as the convective envelope is quickly spun down on the ZAMS, angular momentum is tapped within the inner radiative core and resurfaces later on the MS. However, Jones et al. (1997) quote a 5 km s^{-1} uncertainty in their $v\sin i$ measurements for stars in M34 and all the stars in the 10–20 km s^{-1} bin have a $v\sin i$ less than 12 km s^{-1}, so that the fractional number of stars below and above the 10 km s^{-1} limit is uncertain. At the slightly older age of 300 Myr, Soderblom & Mayor (1993) found all the G-type stars of the UMa Group they surveyed to have projected velocities less than 10 km s^{-1}. Finally, by the age of the Hyades, all stars have converged down to velocities

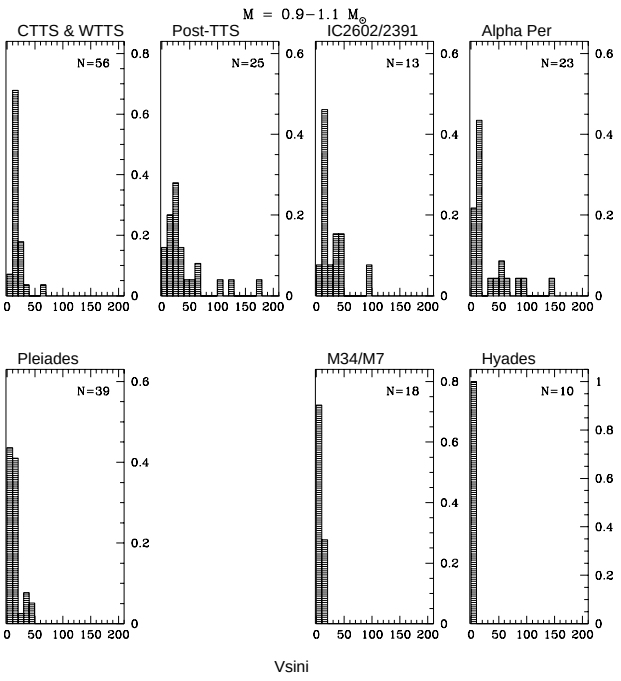

Fig. 8. Observed $v\sin i$ distributions for PMS stars, and stars in young, intermediate-age and old clusters in the mass range 0.9–1.1 $M_\odot$.

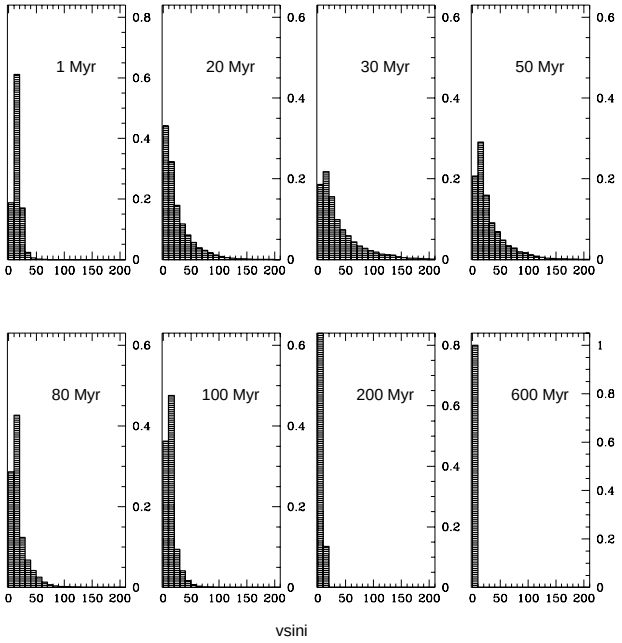

Fig. 9. Synthetic $v\sin i$ distributions at various ages from the 1.0 $M_\odot$ model.

(much) less than 10 km s^{-1}. We will show below (see 6.4) that the rotational periods predicted by the model for 1$M_\odot$ Hyades stars are in excellent agreement with observations.

This quantitative comparison shows that the model reproduces reasonably well the observations all the way from the birthline to the age of the Sun when uncertainties on $v\sin i$ and biases affecting some samples are taken into account. There is, however, a noticeable difference between model and observed distributions. The observed distributions usually exhibit a peak at low velocities and a flat high-velocity tail, while the model distributions are much "smoother" with an excess of intermediate rotators (30–50 km s^{-1}) compared to observations. This difference in shape between model and observed distributions directly stems from the form of the distribution of disk lifetime that we considered, i.e., $\tau_{disk} \propto 1/t$. With this distribution, the fraction of stars that uncouple from their disk is directly proportional to $\log t$. This simple distribution naturally leads to a very smooth and continuous $v\sin i$ distribution at all ages which peaks at low velocity and steadily decreases towards high rotators. A better match to the shape of the observed distributions could have been obtained using more sophisticated forms of the disk lifetime distribution. We did not attempt to define such distributions, however, as we feel that this would introduce too much "fine tuning" of the model in regard to the currently available constraints on disk lifetimes. Indeed, it is not as important to reproduce the exact shape of the observed $v\sin i$ distributions than to account for the extent of their high-velocity tail and for the fraction of slow rotators they contain. As discussed above, these two aspects of the $v\sin i$ distributions are directly related to the relative fraction of short- and long-lived disks and to the assumptions made for angular momentum loss. That the model accounts for these two fundamental aspects of the $v\sin i$ distributions is considered to be sufficient pending additional observational constraints.

6.2. 0.8 $M_\odot$ model

The rotational evolution of lower mass stars cannot be describe with the same set of parameters than that used for 1$M_\odot$ stars for 2 reasons. Firstly, lower mass stars have a lower moment of inertia and will therefore be more efficiently braked than higher mass stars. Secondly, lower mass stars have a longer contraction timescale to the ZAMS (Fig. 1). Therefore, they will not spin up as quickly as higher mass stars. As a result, lower mass stars do not reach as high velocities at the age of young open clusters than do higher mass stars. However, observations indicate that velocities of the order of 200 km s^{-1} are present in young cluster dwarfs over a wide range of masses. Then, in order to compensate for the less efficient spin up of low mass stars during their PMS evolution, one has to reduce the amount of PMS angular momentum losses they experience (Barnes & Sofia 1996). For 0.8$M_\odot$ models, we therefore adopt a saturation velocity of 8$\Omega_\odot$, instead of 14$\Omega_\odot$ for 1$M_\odot$ stars (Fig. 3). The braking law remains the same at low velocity but is a factor of $(8/14)^{-2}$ = 3 weaker than for 1$M_\odot$ stars in the saturated regime. The different saturation velocity used for lower mass stars is the only one parameter that changes from one model to the other. All other parameters (initial distribution of rotational periods, disk lifetime distributions, calibration constant of the braking law) remain the same.

The observed distributions of linear velocities are shown in Fig. 10 and the synthetic ones computed from the model are

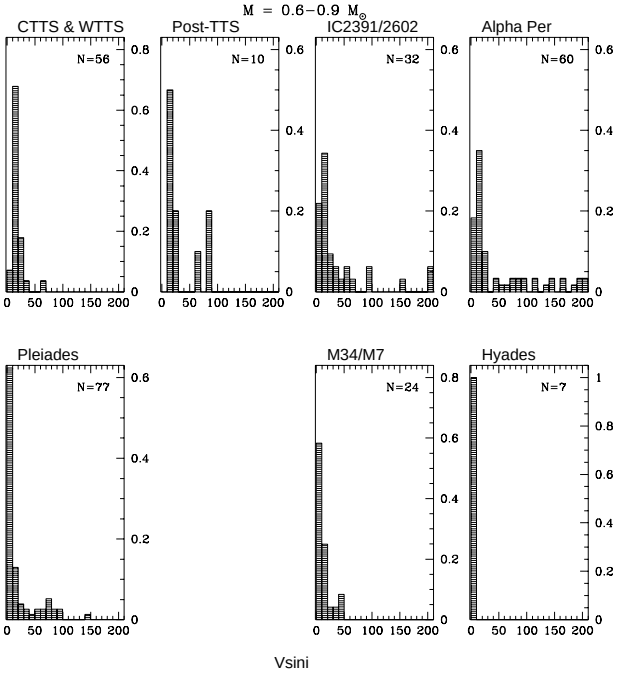

Fig. 10. Same as Fig. 8 for stars in the mass range 0.6–0.9 $M_\odot$.

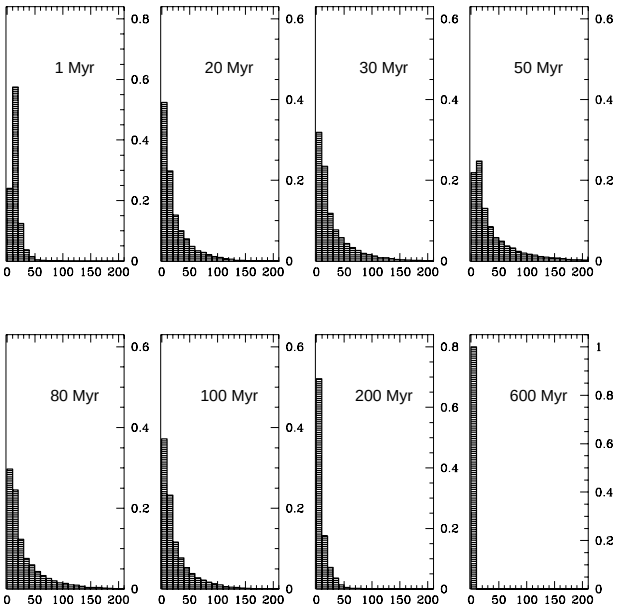

Fig. 11. Same as Fig. 9 from the 0.8 $M_\odot$ model.

shown in Fig. 11. The model predicts that the maximum velocities, of the order of 200 km s^{-1}, are reached at an age of 50 Myr, slightly before 0.8$M_\odot$ stars settle on the ZAMS. For 1$M_\odot$ stars, peak velocities are reached earlier, at an age 30 Myr. The time delay in reaching peak velocities for lower mass stars is a direct consequence of both their longer contraction timescale to the ZAMS, and the weaker braking law in the saturation regime. Hence, the model predicts that the ratio of fast to slow rotators is the largest at an age of 50 Myr for 0.8$M_\odot$, in agreement with the $v\sin i$ distribution of 0.8$M_\odot$ stars in the Alpha Persei cluster.

Observations suggest that most of the fast rotators are subsequently very rapidly braked on the ZAMS and that by the age of the Pleiades more than 60% of the stars are very slow rotators with $v\sin i$ less than 10 km s^{-1}. Yet, the model predicts only a fraction of 30–40% of such slow rotators at an age between 80 and 100 Myr, even though the maximum velocities predicted by the model (100–150 km s^{-1}) agree with observations and do indicate that 0.8$M_\odot$ stars have been spun down between the age of the Alpha Persei cluster and the age of the Pleiades cluster. Even without any reference to models, the large fraction of very slow rotators observed in the Pleiades is puzzling. For both higher and lower mass stars, the frequency of slow rotators steadily increases from 50 to 600 Myr in open clusters, as can be expected from ZAMS spin down. In contrast, for 0.8$M_\odot$ stars, observations suggest that the relative number of slow rotators increases between Alpha Per and the Pleiades, as expected, but decreases from the Pleiades to the older M34 cluster. Such a behaviour could be expected from the entrainement of the slowly rotating outer convective envelope by a rapidly spinning radiative core, which would then imply large internal differential rotation. However, resurfacing of angular momentum tapped into the radiative core during ZAMS evolution should be more important for higher mass stars since they have a larger radiative core, which is not observed. On the other hand, it seems difficult to blame the observations which are numerous for stars in this mass range both in the Pleiades and Alpha persei clusters and thus leave little room for statistical fluctuations.

Later on the ZAMS, the 200 Myr M34 cluster still exhibits a few rapid rotators with a velocity up to 50 km s^{-1} which indicates that lower mass stars have longer spin down timescales than 1$M_\odot$. At this age, the synthetic and observed distributions are in good agreement. The longer spin down timescale predicted from the model for lower mass stars is the result of the weaker angular momentum losses they experience in the saturated regime (see Fig. 7). Finally, by the age of the Hyades, all 0.8$M_\odot$ stars have been braked to velocities less than 10 km s^{-1}. In summary, the major features of the evolution of low mass stars compared to 1$M_\odot$ stars, i.e.: longer spin up timescale, similar ultrafast velocities at the ZAMS, longer spin down timescale, are all accounted for by only allowing for weaker angular momentum losses in the saturated regime compared to higher mass stars.

6.3. 0.5 $M_\odot$ model

Observationally, the trends outlined above for 0.8$M_\odot$ stars are even more pronounced for 0.5$M_\odot$ stars, although only Pleiades and Hyades have significant samples of stars with known $v\sin i$ in this mass range (see Fig. 12). A clear difference in the $v\sin i$ distribution of 0.5$M_\odot$ stars compared to higher mass stars is apparent in both clusters: the fraction of slow rotators in the Pleiades is much lower than for higher mass stars, and there are still a number of significant rotators ($v\sin i$>10 km s^{-1}) in the Hyades, which indicates a spin down timescale for the lowest mass stars of the order of the Hyades age (600 Myr). The same arguments used in the previous sections for 0.8$M_\odot$ stars apply

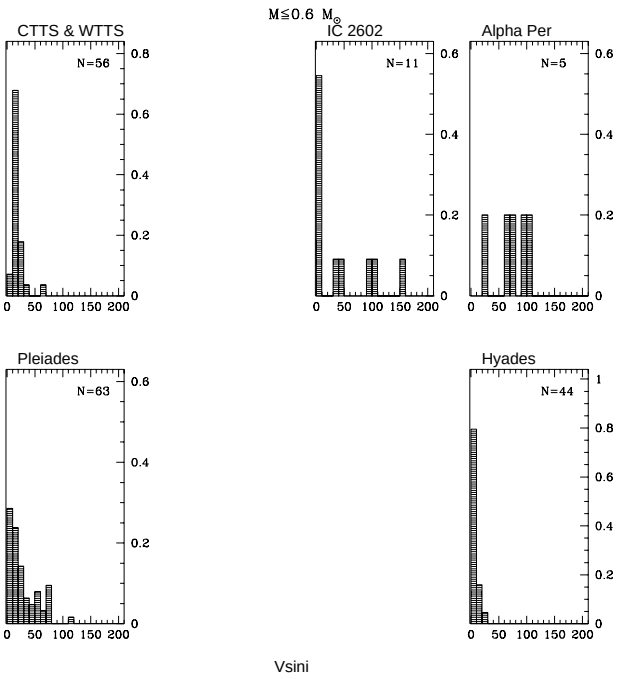

Fig. 12. Same as Fig. 8 for stars less massive than 0.6 $M_\odot$.

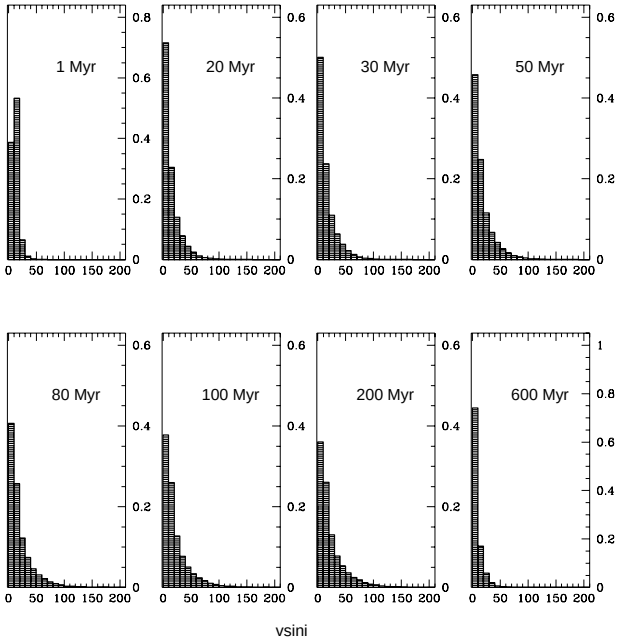

Fig. 13. Same as Fig. 9 from the 0.5 $M_\odot$ model.

again for 0.5$M_\odot$ stars: in order to reach fast velocity in young open clusters in spite of a less efficient PMS spin up, the angular momentum losses experienced by the lowest mass stars must be correspondingly decreases. In the model presented in Fig. 13, the saturation velocity is reduced to $3\Omega_\odot$ (see Fig. 3).

Stars with a mass around 0.5$M_\odot$ reach the ZAMS at an age of 200 Myr. Therefore, at the age of the Pleiades, they are still in their PMS contraction phase, while higher mass stars have already started their spin down phase on the ZAMS. This explains why the observed fraction of very slow rotators in this mass range is so small at an age of 70–100 Myr. In fact, the model predicts a slight excess of slow rotators compared to the observations at the age of the Pleiades. This excess can be traced back to a corresponding excess of slow rotators in the model distribution of T Tauri stars. By changing the initial conditions and assuming an average rotational period of 5 days instead of 8 days for the least massive T Tauri stars, the model distributions would better agree with the observed ones at the T Tauri stage and at the age of the Pleiades. Even though there is little observational evidence for a shorter average rotational period in the least massive T Tauri stars, some very low-mass T Tauri stars do seem to exhibit significant rotational velocities (see Bouvier 1991, Fig. 4).

The model suggests that peak velocities of $\simeq 120\,\mathrm{km\,s^{-1}}$ will be reached at an age of about 200 Myr, a prediction which could be tested by measuring the $v\sin i$ of the lowest mass stars in intermediate-age open clusters. Because of the long timescales involved for both PMS spin up and ZAMS spin down of such low mass stars,there is little evolution of the $v\sin i$ distribution between 50 and 200 Myr, and the maximum model velocities at the age of the Pleiades ($\simeq 100\,\mathrm{km\,s^{-1}}$) are already close to the peak velocities reached by 0.5$M_\odot$ stars during their evolution.

The major difference between 0.5$M_\odot$ stars and higher mass ones is the existence of rotators with $v\sin i$ above $10\,\mathrm{km\,s^{-1}}$ by the age of the Hyades (Stauffer et al. 1997a). The model and observed distributions are quite similar at 600 Myr, which suggests that the combination of long contraction timescale to the ZAMS and, more importantly, the much weaker angular momentum losses experienced by the lowest mass stars allow fast rotators to survive up to the age of the old Hyades cluster. We return to a detailed comparison between the predicted and observed rotational distribution of the Hyades low-mass dwarfs in the next section.

6.4. Rotational period distribution at the age of the Hyades

Hyades is the only open cluster where a tight relationship between rotational period and stellar mass has been found so far (Radick et al. 1987). In the mass range from 0.6 to 1.1$M_\odot$, Hyades dwarfs exhibit narrow rotational period distributions with a mean rotational period shortening with increasing mass. This tight rotation-mass relationship in such an old cluster results from the convergence of the rotation rates of late-type stars down to low velocities as they age on the main sequence. For Hyades stars less massive than 0.6$M_\odot$, however, the dispersion of the P_{rot} distribution suddenly increases, which reflects the much longer timescale needed for the lowest mass stars to spin down on the main sequence.

Fig. 14 shows the synthetic distributions of rotational periods at the age of the Hyades (600 Myr) predicted by the models for 1.0, 0.8, 0.6 and 0.5$M_\odot$ stars. For the higher mass stars, the distributions are narrow and tend to widen toward lower masses. The average rotational periods range from 8–9 d for 1$M_\odot$ stars,

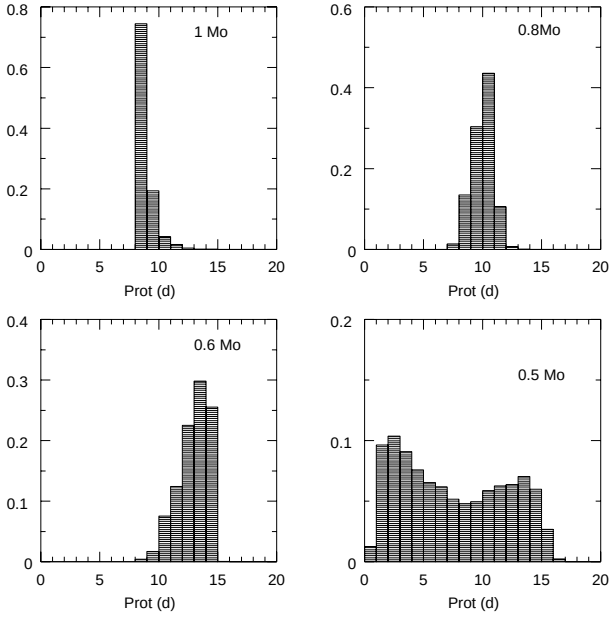

Fig. 14. Synthetic distributions of rotational periods as predicted from the models for 1.0, 0.8, 0.6 and 0.5$M_\odot$ stars at the age of the Hyades.

to 10–11 d for 0.8$M_\odot$ stars and 13–14 days for 0.6$M_\odot$ stars. Both the average periods, the width of the distributions and their variations with stellar mass compare very well with the rotation-mass relationship found by Radick et al. (1987, see their Fig. 4a). The lowest mass stars in the Hyades are predicted to have a much wider period distribution, extending all the way from less than 1d up to 15d. The only rotational period measured by Radick et al. (1987) in this mass range amounts to 3.66d. Converting the synthetic rotational period distribution of the lowest mass stars into rotational velocities, one obtains a distribution of V_{eq} which strongly peaks at very low velocities (80% of the stars have V_{eq} less than 8 km s^{-1}) with a tail of rotators extending up to 30 km s^{-1}. Such a synthetic distribution of V_{eq} is in excellent agreement with the recently derived distribution of $v\sin i$ for the lowest Hyades stars by Stauffer et al. (1997a).

6.5. Summary

The models presented above account for the most salient features of the angular momentum evolution of low-mass stars from the time they appear in the HR diagram as T Tauri stars up to the age of the Sun. The reduction of the moment of inertia leads to rapid spin up during the pre-main sequence, which accounts for the existence of the ultrafast rotators in the young open clusters. Simultaneously, young stars that are prevented from spinning up due to the interaction with their long-lived disks are the progenitors of the numerous intermediate and slow rotators on the ZAMS. Once they have settled on the ZAMS, all stars spin down at a rate which depends upon their mass due to the angular momentum carried away by their solar-type magnetized wind. In these models, the longer spin down timescale for lower mass stars primarily results from the lesser efficiency of magnetic braking and, to a lesser extend, from the fact that lower mass stars have longer contraction (i.e., spin up) timescale to the ZAMS.

7. Discussion

The models of angular momentum evolution proposed so far in the literature can be divided in 3 broad classes which differ primarily by the assumptions made regarding angular momentum transport in the stellar interior. The models presented here assume complete redistribution of angular momentum on a timescale much shorter than the evolutionary timescale (see also Collier Cameron & Li 1994). Another class of models have used the timescale for internal momentum transport as a free parameter to be adjusted so as to provide "best fit" models to the observations (MacGregor & Brenner 1991, Keppens et al. 1995). In a related model, Strom (1994) suggested that angular momentum is locally conserved in contracting PMS stars. However, angular momentum losses were neglected, which would prevent the stars from reaching high velocities on the ZAMS. Both classes of models are phenomenological in the sense that the internal redistribution of angular momentum is either postulated, as here, or parametrized. The third class of models attempt to include a physical description of this process. The Yale models for instance (Pinsonneault et al. 1989, Krishnamurthi et al. 1997), treat as a diffusion process the redistribution of internal angular momentum by hydrodynamical instabilities acting on both dynamical and secular timescales. Apart from this important difference, all models include similar stellar evolutionary codes in order to estimate structural changes occuring in the star as it evolves, as well as qualitatively similar "saturated" braking laws, although the amplitude of the angular momentum losses may greatly vary from one model to the other. As a result, the debate on angular momentum evolution of low-mass stars has recently focused onto the issue of the timescale for angular momentum transport in stellar interiors (e.g., Li & Collier Cameron 1993), which we address below.

Major uncertainties still remain regarding the dominant mechanisms responsible for the transport of angular momentum in radiative interiors (see, e.g., Charbonneau 1992 and Zahn 1992). Pinsonneault et al. (1989), and subsequent models by the Yale group, assumed that angular momentum is transported through the development of various hydrodynamical instabilities, and included in their model a set of radial diffusion equations in order to describe these processes. In these models, angular momentum transport is dominated by secular instabilities which act on a timescale comparable to evolutionary timescales. As a result, these models have some difficulties in predicting a rotational profile consistent with the nearly uniform rotation of the Sun, as suggested by helioseismology results (Pinsonneault et al. 1989, Krishnamurthi et al. 1997, Chaboyer et al. 1995). Alternatively, Zahn et al. (1997) claimed that only gravity waves are efficient enough in transporting angular momentum so as to account for the Sun's flat rotational profile (see also Kumar & Quataert 1997). And Charbonneau & McGregor (1993) argued that transport by magnetic torques may also be important

in understanding the helioseismology results, which to date are the only available constraint on transport theories. Zahn et al. (1997) derived a characteristic timescale of 10^7 yr for angular momentum redistribution by gravity waves, while Charbonneau & MacGregor (1993) suggested a timescale as short as a few 10^6 yr from MHD processes, depending on the topology of the magnetic field inside the star. Both mechanisms thus yield strongly enhanced angular momentum transport compared to secular hydrodynamical instabilities and seem to be required to account for the quasi-solid body rotation of the inner Sun. Our assumption of nearly solid body rotation would indeed support very efficient mechanisms for internal angular momentum transport.

The main consequence of the assumption that the star is rotating nearly as a solid-body is that long disk lifetimes are required to account for the slow rotators in young open clusters. The "best fit" models presented above assume a distribution of disk lifetime which is log-uniform, with a maximum lifetime of 40 Myr. This distribution implies that as much as 20% of stars are still surrounded by, and interacting with, their disk at an age of 10 Myr, a fraction which decreases to 10% at an age of 20 Myr. We have already discussed above the empirical estimates of disk lifetimes drawn from surveys of near-IR excess among PMS stars (see 3.4) and concluded that the model distribution is not inconsistent with the most recent estimates, though it uncomfortably lies at the higher limits of the IR-excess frequency distribution. There is no direct observational support for disk lifetimes as long as 20 Myr. Whether the lack of observational evidence rules out such long disk lifetimes for a small fraction of stars is, however, unclear. Firstly, most stars in dark clouds have an age much less than 10 Myr (Kenyon & Hartmann 1995, Strom 1995, Lawson et al. 1996). Lacking a significant population of PMS stars older than 10 Myr, one cannot derive estimates of disk frequency from the distribution of near-IR excess among PMS stars on their radiative tracks. The controversial discovery of many post-T Tauri stars (PTTS) in this age range, from ROSAT and follow-up spectroscopic observations (e.g., Wichmann et al. 1996), does not help either. Because the PTTS samples are X-ray selected, only fast rotators are detected, which have already dissipated their disk and therefore are not expected to exhibit any IR excess (Bouvier et al. 1997a, Wichmann et al. 1997b).

Secondly, as the disk evolves and ultimately dissipates, the observational diagnostics of disk accretion become increasingly difficult to observe. Current work on accretion disk diagnostics suggests that only mass-accretion rates larger than about $10^{-9}M_\odot yr^{-1}$ yield detectable accretion signatures (UV excess, optical veiling, Balmer line emission) in the spectra of young stars (Basri & Bertout 1989, Hartigan et al. 1995). Armitage & Clarke (1997) also argued that CTTS magnetically coupled to their disk would lack a detectable near-IR excess for a mass-accretion rate below $10^{-8}M_\odot yr^{-1}$ as the star's magnetosphere disrupts the inner disk up to the corotation radius. According to Cameron & Campbell's (1993) and Armitage & Clarke's (1996) star-disk coupling models, disk locking remains effective down to mass accretion rates of a few $10^{-11}M_\odot yr^{-1}$. Therefore, there exists a wide range of mass accretion rates, from 10^{-11} to $10^{-9}M_\odot yr^{-1}$, for which the star's rotation can still be regulated by the star-disk interaction but with spectral signature of disk accretion that are too faint to be detected. The evolution of the dust content, which is responsible for the far-IR and millimetric excesses, is more difficult to predict since it not only depends upon the disk's surface density but also upon the properties of dust grains (e.g. Henning & Stognienko 1996, Mannings & Emerson 1994). The sudden transition from optically thick to optically thin disks, which occurs on a timescale of about 10^5 yr (Strom et al. 1989, Kenyon & Hartmann 1995), can be interpreted either as an actual decrease in surface density, suggesting that the disk is rapidly depleted (Skrutskie et al. 1990, Armitage & Clarke 1997) or, alternatively, as rapidly changing dust properties due to, e.g., grain growth by coagulation on a timescale of a few 10^4–10^5 yr (Ruden & Pollack 1991, Stepinski & Valageas 1996a,b, Wolk & Walter 1996). In the latter case, the lack of an observable IR excess could result from the lower opacity of larger dust grains and does not necessarily point to the end of the accretion phase. The tight relationships found between the amplitude of dust-related and gas-related diagnostics of accretion nevertheless suggests that the evolution of dust in circumstellar disks closely follows that of the gas (Edwards et al. 1993b, Hartigan et al. 1995). Hopefully, observations of large samples of young stars in the mid- and far-IR range with the ISO satellite will clarify the evolution of dust grains in circumstellar disks.

The distribution of disk lifetimes can be traced back to the distribution of initial disk masses. Armitage & Clarke (1996) followed the temporal evolution of gaseous circumstellar disks during the pre-main sequence and found that star-disk decoupling occurs at an age of about 10^7 yr for an initial disk mass between $3\ 10^{-3}$ to $10^{-1}M_\odot$. They predict rotational periods of the order of 4 days on the ZAMS, which corresponds to equatorial velocities of 12 km s^{-1} for $1M_\odot$ stars, reasonably consistent with the projected velocities measured for slow rotators in young open clusters. Cameron et al. (1995) derived similar results and suggested that stars born with massive disks remain coupled for most of their PMS evolution and thus arrive on the ZAMS as slow rotators. In this framework, the distribution of disk lifetimes used here would suggest that the 20% of stars that are still coupled to their disk at an age of 10^7 yr were born with the most massive circumstellar disks or envelopes ($\simeq 0.1M_\odot$, André & Montmerle 1994).

Krishnamurthi et al. (1997) recently argued that disk lifetimes significantly shorter than 10 Myr could still lead to slow rotators on the ZAMS provided that the assumption of solid body rotation be relaxed. If differential rotation is allowed, the angular momentum losses at the stellar surface affect preferentially the outer convective zone, and only slowly propagate through the stellar interior. Therefore, for a given amount of angular momentum loss at the stellar surface, the photosphere of a differentially rotating star will be braked faster than that of a solid-body. As an extreme example, one may consider a star whose convective envelope is totally decoupled dynamically from the radiative core. Then, a small amount of angular momentum loss at the surface would be very efficient in braking the star's outer layers, because only the convective envelope, which

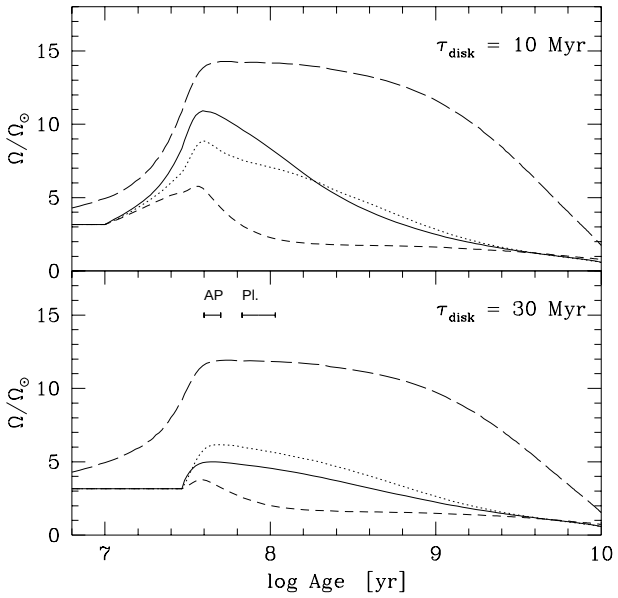

Fig. 15. Surface and core velocity of $1M_\odot$ slow rotators with and without core-envelope decoupling. The core-envelope coupling timescales (τ_c) are 10^6 yr (equivalent to solid-body rotation, solid line), 2 10^7 yr (dotted line), and 5 10^8 yr (short dashed line). Two disk lifetimes are illustrated: 10 Myr (top panel) and 30 Myr (lower panel). The long-dashed curves show the velocity of the core for core-envelope coupling timescales of 5 10^8 yr. All models were calibrated so as to reproduce the solar rotational velocity at the age of the Sun (Allain, in prep.). The calibration varies with τ_c but is independent of τ_{disk}. For a disk lifetime of 10 Myr, DR models with τ_c of 10 Myr predict slightly lower velocities than SB models on the ZAMS. For a disk lifetime of 30 Myr, DR models with τ_c of 10 Myr predict higher velocities than SB models at the age of the young clusters as angular momentum tapped into the inner radiative core resurfaces. By increasing τ_c up to a few 10^8 yr, very slow surface velocities are reached on the ZAMS but the radiative core remains in rapid rotation past the age of the Sun.

has a low moment of inertia compared to the entire star, has to be braked ($\tau_J \propto I_{conv} << I_{tot}$). At the other extreme, solid-body rotation implies a perfect dynamical coupling between the convective envelope and the radiative core, so that the entire star has to be braked, which happens on a longer timescale. Hence, the timescale for braking the stellar surface is longer for solid-body rotation (SB) models than for differential rotation (DR) ones. Consequently, in order to reproduce the slow rotators on the ZAMS, SB models ought to require longer disk lifetimes, so that the duration of the pre-ZAMS spin up phase is shortened, thus compensating for the lesser efficiency of the wind braking compared to DR models.

It must be stressed, however, that partial decoupling between the radiative core and the convective envelope does not actually allow for a substantial reduction of disk lifetimes *unless the coupling timescale between the core and the envelope is assumed to be very long* ($>>$ 10 Myr). For instance, Keppens et al.'s (1995) model assumes a core-envelope coupling timescale of 10 Myr. With maximum disk lifetimes of 6 Myr, they find that no slow rotators ($v\sin i \leq 10\,\mathrm{km\,s^{-1}}$) are predicted at an age of 50 Myr. In order to account for the slow rotators at this age, their model would have to include longer disk lifetimes, not very different from those assumed by SB models. This occurs because, even though the braking of surface layers is more efficient, the relative reduction of the moment of inertia of the convective envelope alone is larger than that of the whole star just before the ZAMS (see Keppens et al.'s Fig. 2). As a result, the decoupled convective envelope tends to spin up faster than the whole star just before reaching the ZAMS. More importantly, because the core-envelope coupling timescale is of the order of the contraction timescale to the ZAMS (10–20 and 30–40 Myr, respectively), significant amount of angular momentum tapped into the radiative core is transported to the envelope before the star reaches the age of the Pleiades. These two effects are illustrated in Fig. 15 where we compare slowly-rotating $1M_\odot$ models for solid-body rotators to models with core-envelope decoupling following Keppens et al.'s prescription for angular momentum transfer between the core and the envelope (Allain, in prep.). It is seen that unless the timescale for core-envelope coupling becomes very long ($>>$ 10^7 yr), DR and SB models predict roughly similar velocities at an age of 30–80 Myr. For a τ_{disk} of 10 Myr, DR models with a τ_c of 20 Myr predict rotational velocities of 15 km s^{-1} at the age of the Pleiades, compared to 18 km s^{-1} for SB models. Only very long coupling timescales between the core and the envelope ($\simeq$ 100 Myr, e.g., Krishnamurthi et al. 1997) would produce very slow rotators with significantly shorter disk lifetimes. While this might well be the case for very slow rotators in young clusters, such a long coupling timescale fails to reproduce the ultrafast rotators, as the convective envelope is very efficiently braked before the stars reach the ZAMS (see Charbonneau et al. 1995), and also still exhibit significant differential rotation at the age of the Sun, which conflicts with the results from helioseismology.

Originally, the core-envelope decoupling assumption was called upon in order to account for i) the rapid spin down of fast rotators on the ZAMS (Endal & Sofia 1981) and ii) the mass-dependence of the ZAMS spin down timescale, being longer for lower mass stars (Stauffer et al. 1985). The results obtained from the SB models above show that these two characteristic features of the rotational evolution of low-mass stars may have other causes. The rapid spin down of fast rotators on the ZAMS does not require the core-envelope decoupling hypothesis. Instead, the fast spin down of the whole star in SB models occurs at a rate consistent with the observations solely on the basis of the adopted braking law. And the longer spin down timescale for lower mass stars in the SB models is explained by the mass-dependent saturation of the angular momentum losses, which occurs at lower velocities for lower mass stars, as suggested earlier by Collier Cameron & Li (1994). This mass-dependency is expected on a physical basis in the framework of the $\alpha - \omega$ dynamo model. The amplification of seed magnetic fields by the dynamo process scales as the inverse of the Rossby number, $R_o^{-1} \propto \omega\tau_{conv}$, where τ_{conv} is the convective turnover time. Assuming that the saturation of the angular momentum losses is a direct consequence of the saturation of the dynamo itself, it is expected to occur at a fixed R_o^{-1} for all masses. There-

fore, since τ_{conv} increases with decreasing stellar mass, ω_{sat} is a decreasing function of stellar mass. The relative values of ω_{sat} empirically obtained from the best fit models above (14, 8 and $3\Omega_\odot$ for 1.0, 0.8 and $0.5M_\odot$ models, respectively) indeed closely match the run of $(\tau_{conv})^{-1}$ with stellar mass (see also Patten & Simon 1996, Barnes & Sofia 1996, Krishnamurthi et al. 1997) and their absolute values are consistent with the saturation velocities derived from activity-rotation relationships (15–25 km s^{-1} for $1M_\odot$ stars, e.g., Stauffer et al. 1994). Alternatively, Giampapa et al. (1996) have suggested on the basis of the X-ray spectra of the lowest-mass stars that fully convective stars have complex magnetic field geometries, which mostly consist of small closed loops that contribute little to angular momentum loss. The changing magnetic field geometry, with an increasing number of closed loops, towards lower mass stars could also lead to a mass-dependent saturation of the angular momenum losses, thus mimicking a saturation of the dynamo process.

In the light of the new SB models, the early motivations for introducing the assumption of core-envelope decoupling may not appear as necessary. Since then, however, two other arguments in favor of core-envelope decoupling have been put forward. One is based on the observations of significant rotation rates among horizontal-branch stars in globular clusters (Peterson 1985). The interpretation is that angular momentum has been tapped into a rapidly rotating core on the main sequence and resurfaces as the star evolves off the main sequence, thus accounting for post-MS spin up in spite of the increasing stellar moment of inertia. Such an interpretation, however, requires that the coupling timescale between the core and the envelope be comparable to or longer than the main sequence lifetime of solar-mass stars, i.e., $\simeq 10^{10}$ yr. As discussed above, such a long coupling timescale leads to other difficulties in the models. Therefore, the rotation rates of these evolved stars remain a puzzle which can be explained neither by current (solar metallicity) SB nor DR models, and may point to the role of metallicity in the stars' rotational history (Pinsonneault et al. 1991). The vast majority of Pop.I low-mass giants and subgiants have extremely low surface velocities indeed (De Medeiros et al. 1996) and Schrijver & Pols (1993) argued that their rotational evolution off the main sequence was best understood by assuming a very efficient redistribution of angular momentum, on a timescale of less than 5 Myr. The other argument is based on the rotational evolution of slow rotators on the ZAMS. Krishnamurthi et al. (1997) correctly pointed out that the braking timescale for slow rotators on the ZAMS is very long in SB models (see Fig. 6). They claim that the decreasing velocity of slow rotators between the Alpha Persei and Pleiades clusters indicate that even the slowest rotators experience significant braking on the ZAMS, therefore suggestive of core-envelope decoupling. Their analysis, however, is flawed by the inclusion of numerous $v\sin i$ *upper limits* in the slow rotator data that the authors consider as actual $v\sin i$ measurements in their binned distribution of $v\sin i$. In order to determine whether the slowest rotators do lose angular momentum at a significant rate on the ZAMS, one has to investigate the evolution of the *lower envelope* of the rotational velocity distribution. This cannot be done from the currently uncomplete $v\sin i$ distributions, which include numerous upper limits of 7 to 10 km s^{-1} for slow rotators. And rotational period measurements in young clusters are still too sparse to infer precise minimum rotation rates (e.g., Allain et al. 1996, Prosser & Grankin 1997). Therefore, the rate at which the slowest rotators are braked on the ZAMS between 50 and 70–100 Myr currently remains uncertain. Actual $v\sin i$ measurements of the slowest rotators in young clusters are needed to better constrain their evolution on the ZAMS.

More recently, however, Stauffer et al. (1997b) claimed to have obtained resolved $v\sin i$ measurements for an unbiased sample of G stars in the IC 2391 and IC 2602 clusters, at an age of 30 Myr. Comparing their $v\sin i$ distribution to that of the Pleiades G dwarfs, they concluded that slow rotators must lose half of their angular momentum between 30 Myr ($v\sin i$=20 km s^{-1}) and 70 Myr ($v\sin i$=10 km s^{-1}) if they rotate as solid bodies. The braking law used in the $1M_\odot$ SB model above predicts a reduction by only 30% in the angular momentum of slow rotators during this time span. Thus, unlike fast rotators, very slow rotators may experience core-envelope decoupling on the ZAMS. For rapid rotators, Stauffer et al. found a reduction by a factor of 2 in $v\sin i$ between the age of IC clusters and that of the Pleiades. The illustration of rotational tracks for $1M_\odot$ SB models (see Fig. 4) indicate a similar amount of spin down during early ZAMS evolution.

Although one still has to wait a decade or so before space-born stellar seismology reveals the state of internal rotation in solar-mass ZAMS stars, some insight can already be obtained from the activity-rotation relationships observed for these stars. ROSAT studies of young open clusters have shown that the X-ray luminosity of low-mass dwarfs is mainly determined by their surface rotational velocities, with the fastest rotators being the brightest X-ray sources (Stauffer et al. 1994, 1997b, Randich et al. 1996, Prosser et al. 1996). In particular, there exist a tight relationship between the level of coronal activity and both the rotational period and the Rossby number for late-F to M stars in young clusters, where the X-ray luminosity steadily decreases with increasing rotational periods between 2 and 10 days (Randich et al. 1996, Patten & Simon 1996, Stauffer et al. 1997b). These relationships are expected in the framework of the $\alpha-\omega$ dynamo model *if* internal differential rotation scales with surface rotation (Durney & Latour 1978). Indeed, it is not surface rotation but internal differential rotation that drives the dynamo. The core-envelope decoupling models, however, predict quite a different relationship between surface rotation and internal differential rotation. As the outer convective zone is rapidly braked on the ZAMS, the radiative core remains in rapid rotation. Therefore, slow rotators with rapidly rotating cores have a large gradient of internal rotation at the core-envelope interface, which is thought to be the locus where the dynamo operates. A very efficient dynamo should consequently result leading to a high level of coronal and chromospheric activity. Such slowly rotating stars (i.e., stars with long rotational periods or large Rossby numbers) exhibiting high activity levels would easily be detected from ROSAT studies and are actually not observed.

8. Conclusion

The issue of angular momentum transport in stellar interiors is far from being solved. Nevertheless, the comparison of models predictions with observations provide some insights. We have shown that solid-body models can reproduce reasonably well the evolution of the surface rotation rates of *moderate and fast rotators*, which is well constrained by observations from the T Tauri phase up to the age of the Sun, in the mass range 0.5–1.1$M_\odot$. This result suggests that angular momentum transport is quite efficient in the radiative interiors of fast rotators, acting on a timescale much shorter than evolutionary ones. In agreement with other recent models, SB models also suggest that the angular momentum loss rate at the stellar surface saturates at high surface velocity with a mass-dependency which may be related to the efficiency of the dynamo process itself.

In contrast, no firm conclusions can be drawn at this point for the evolution of *very slow rotators* on the ZAMS: lacking precise measurements of their rotation rate, observations provide little constraints on the timescale for internal angular momentum redistribution in these stars. Work in progress to measure the $v\sin i$ of slow rotators in young clusters (Allain et al. 1997, Queloz et al. 1997) ought to provide an estimate of their braking timescale on the ZAMS, for which SB and DR models make different predictions.

The models presented here imply accretion disk lifetimes ranging from a few 0.1 up to a few 10 Myr, with an median lifetime of 3 Myr. The shortest disk lifetimes allow for the PMS spin up of ultra-fast rotators to the ZAMS, which are better accounted for by SB models than by core-envelope decoupling ones. The longest disk lifetimes of a few 10 Myr are required to account for the slowest rotators in young clusters, assuming solid-body rotation. However, if the timescale for angular momentum redistribution turned out to be longer than about 100 Myr in ultra-slow rotators, shorter maximum disk lifetimes would be required. Resolution of this issue awaits the measurement of the rotation rates of the slowest rotators in young clusters.

Appendix

We describe here how we built the observed $v\sin i$ distributions and the sources from which they were taken. Because $v\sin i$ measurements are still much more numerous than determinations of rotational periods, we did not attempt to include the latter in the rotational distributions. Known spectroscopic binaries have been discarded.

CTTS and WTTS ($\simeq$ 1Myr): all stars with a mass less than 1.2$M_\odot$ and an age less than 5 Myr were considered. Most stars have an age of about 1 Myr. The stellar mass and age were deduced from the star's location in the HR diagram. The $v\sin i$ measurements are from: Bouvier et al. (1986), Bouvier (1990), Hartmann et al. (1987), Hartmann & Stauffer (1989), and Walter et al. (1988). In most studies, the resolution limit is 10 km s^{-1}.

For older stars, $v\sin i$ distributions were built in 3 mass ranges: 0.9–1.1, 0.6–0.9, $\leq$0.6$M_\odot$. The mass and age of PTTS were deduced from their location in the HR diagram. For cluster dwarfs, we used the dereddened (B–V) color as a mass indicator, with the following respective intervals: 0.58–0.77, 0.77–1.24, $\geq$1.24.

Post-TTS ($\simeq$ 10–30 Myr): the $v\sin i$ data for PMS stars with an age $\geq$4 Myr (most have an age $\geq$10 Myr) are from Wichmann et al. (1997, ROSAT X-ray sources identified as PTTS in the Lupus region, in prep.) and Covino et al. (1997, ROSAT X-ray sources identified as PTTS in the Chameleon region, in prep.). Preliminary results have been published by Covino et al. (1997). These samples are X-ray selected, introducing a bias against the detection of slow rotators (Bouvier et al. 1997a).

IC 2602/2391 ($\simeq$ 30 Myr): IC 2391 $v\sin i$ measurements are from Stauffer et al. (1989b) and Stauffer et al. (1997b) and the photometry is from Patten & Simon (1996). For IC 2602, the $v\sin i$ data are from Stauffer et al. (1997b) and the photometry from Randich et al. (1995). The stellar samples are X-ray selected and, therefore, possibly biased against slow rotators. The resolution limit ranges from 7 to 10 km s^{-1}.

Alpha Per ($\simeq$ 50 Myr): $v\sin i$ data are from Prosser (1992, 1994) and Stauffer et al. (1989a, 1993). The resolution limit ranges from 7 to 10 km s^{-1}.

Pleiades ($\simeq$ 70–110 Myr): $v\sin i$ data are from Jones et al. (1996), Mermilliod et al. (1997, in prep.), Soderblom et al. (1993), Stauffer & Hartmann (1987), and Stauffer et al. (1984). Preliminary results on the complete $v\sin i$ distribution of late-type members of the cluster have been presented by Allain et al. (1997). The age of the Pleiades has been estimated to lie between 70 and 110 Myr (e.g., Soderblom et al. 1993, Meynet et al. 1993, Basri et al. 1996).

M34, M7 ($\simeq$ 200–250 Myr): $v\sin i$ measurements for M34 are from Jones et al. (1997). The cluster membership is based on a proper-motion study and the authors warn against possible contamination by field stars for the lowest-mass members of the sample. The uncertainty on $v\sin i$ is 5 km s^{-1}. The $v\sin i$ data for M7 are from Prosser et al. (1995). The stellar sample is partly X-ray selected. The $v\sin i$ resolution limit is 10 km s^{-1}.

Hyades ($\simeq$ 600–700 Myr): the $v\sin i$ data were computed from the rotational periods listed in Radick et al. (1987) applying an average projection factor of $\pi/4$. For the lowest mass cluster dwarfs, $v\sin i$ data are from Stauffer et al. (1997a). The resolution limit of the latter study is 6 km s^{-1}.

References

Alcalá J.M., Terranegra L., Wichmann R., et al. 1996, A&AS 119, 7
Alcalá J.M., Krautter J., Covino E., et al. A&A, in press
Alexander D. R., Ferguson J. W. 1994, ApJ, 437, 879
Allain S., Fernández M., Martín E.L., Bouvier J. 1996, A&A 314, 173
Allain S., Bouvier J., Mayor M., et al. 1997, in: 9th Cambridge Workshop on Cool Stars, Stellar Systems, and the Sun, ed.R. Pallavicini, in press
Anders E., Grevesse N. 1989, Geochim. Cosmochim. Acta, 53, 197
André P., Montmerle T. 1994, ApJ 420, 837
Armitage P.J., Clarke C.J. 1996, MNRAS 280, 458
Armitage P.J., Clarke C.J. 1997, MNRAS, in press
Bardou A., Heyvaerts J. 1996, A&A 307, 1009

Barnes S., Sofia S. 1996, ApJ 462, 746
Basri G. 1987, ApJ 316, 377
Basri G., Bertout C. 1989, ApJ 341, 340
Basri G., Marcy G.W., Graham J.R. 1996, ApJ 458, 600
Bertout C. 1989, ARA&A 27, 351
Bertout C., Basri G. Bouvier J. 1988, ApJ 330, 350
Bouvier J. 1990, AJ 99, 946
Bouvier J. 1991, in: Angular Momentum Evolution of Young Stars, eds. S. Catalano, J.R. Stauffer, p.41
Bouvier J., Forestini M. 1994, in: Circumstellar dust disks and planet formation, eds. R. Ferlet, A. Vidal-Madjar, p.347
Bouvier J., Rigaut F., Nadeau D. 1997b, A&A, in press
Bouvier J., Bertout C., Benz W., Mayor M. 1986, A&A 165, 110
Bouvier J., Cabrit S., Fernández M., Martín E.L., Matthews J. 1993, A&A 272, 167
Bouvier J., Covino E., Kovo O., et al. 1995, A&A 299, 89
Bouvier J., Wichmann R., Grankin K., et al. 1997a, A&A, in press
Briceño C., Hartmann L.W., Stauffer J.R., et al. 1997, AJ, in press
Cabrit S., Edwards S., Strom S.E., Strom K.M. 1990, ApJ 354, 687
Camenzind M. 1990, Rev. Mod. Astron., Vol.3
Cameron A.C., Campbell C.G. 1993, A&A 274, 309
Cameron A.C., Campbell C.G. 1995, Quaintrell H. 1995, A&A 298, 133
Casali M.M., Eiroa C. 1996, A&A 306, 427
Caughlan G.R., Fowler W.A. 1988, Atomic Data Nucl. Data Tables, 40, 283
Chaboyer B., Demarque P., Pinsonneault M.H. 1995, ApJ 441, 865
Charbonneau P. 1992, in: 7th Cambridge Workshop on Cool Stars, Stellar Systems and the Sun, eds M.S. Giampapa, J.A. Bookbinder, ASP COnf. Ser., Vol.26, p.416
Charbonneau P., MacGregor K.B. 1993, ApJ 417, 762
Charbonneau P., Shriver C.J., MacGregor K.B. 1995, in: Cosmic Winds and the Heliosphere", eds. J.R. Jokipii, C.P. Sonett, M.S. Giampapa (Tucson: University of Arizona)
Choi P.I., Herbst W. 1996, AJ 111, 283
Collier Cameron A., Li J. 1994, MNRAS 269, 1099
De Medeiros J.R., Da Rocha C., Mayor M. 1996, A&A 314, 499
Doyle J.G. 1996, A&A 307, 162
Durney B.R., Latour J 1978, Geophys. Astrophys. Fluid Dynamics, Vol.9, p.241
Edwards S., Ray T., Mundt R. 1993b, in: Protostars & Planets III, ed. E. Levy and J. Lunine (University of Arizona Press), p.567
Edwards S., Strom S.E., Hartigan P., et al. 1993a, AJ 106, 372
Elsworth Y., Howe R., Isaak G.R., et al. 1995, Nature 376, 669
Endal A.S., Sofia S. 1978, ApJ 220, 279
Endal A.S., Sofia S. 1981, ApJ 243, 625
Feigelson E.D. 1996, ApJ 468, 306
Feigelson E.D., Casanova S., Montmerle T., Guibert J. 1993, ApJ 416, 623
Forestini M. 1994, A&A 285, 473
Giampapa M.S., Rosner R., Kashyap V., et al. 1996, ApJ 463, 707
Gough D.O. 1990, in: Angular Momentum Evolution of Young Stars, eds. S. Catalano, J.R. Stauffer, p.271
Graboske H.C., DeWitt H.E., Grossman A.S., Cooper M.S. 1973, ApJ, 181, 457
Greene T.P., Meyer M.R. 1995, ApJ 450, 233
Hartigan P., Edwards S., Ghandour L. 1995, ApJ 452, 736
Hartigan P., Hartmann L.W., Kenyon S., Strom S.E., Skrutskie M.F. 1990, ApJ 354, 25
Hartmann L.W., Stauffer J.R. 1989, AJ 97, 873
Hartmann L.W., Cassen P., Kenyon S.J. 1997, ApJ 475, 770
Hartmann L.W., Soderblom D.R., Stauffer J.R. 1987, AJ 93, 907
Henning Th., Stognienko R. 1996, A&A 311, 291
Houdebine E.R., Mathioudakis M., Doyle J.G., Foing B.H. 1996, A&A 305, 209
Hubbard, W.B., Lampe, M. 1969, ApJS, 18, 297
Hughes J., Hartigan P., Krautter J., Kelemen J. 1994, AJ 108, 1071
Jones B.F., Fischer D.A., Stauffer J.R. 1996, AJ 112, 1562
Jones B.F., Fischer D., Shetrone M., Soderblom D.R. 1997, preprint
Kawaler S.D. 1988, ApJ 333, 236
Kenyon S.J., Hartmann L.W. 1995, ApJS 101, 117
Keppens R., MacGregor K.B., Charbonneau P. 1995, A&A 294, 469
Kippenhahn R., Weigert A., Hofmeister E. 1968, Methods of Computational Physics, 7, 129
Koester D. 1976, A&A, 52, 415
Königl A. 1991, ApJ 370, L39
Kraft R.P. 1970, in: Spectroscopic Astrophysics, ed. G. Herbig, p.385
Krishnamurthi A., Pinsonneault M.H., Barnes S., Sofia S. 1997, preprint
Kumar P, Quataert E.J. 1997, ApJ 475, L143
Lada C., Alves J., Lada E.A 1996, AJ 111, 1964
Lada C.J., Young E.T., Greene T.P. 1993, ApJ 408, 471
Lada E.A., Bally J., Stark A.A. 1991, ApJ 368, 432
Lawson W.A., Feigelson E.D., Huenemoerder D.P. 1996, MNRAS 280, 1071
Li J., Collier Cameron A. 1993, MNRAS 261, 766
MacGregor K.B., Brenner M. 1991, ApJ 376, 204
MacGregor K.B., Charbonneau P. 1994, in: 8th Cambridge Workshop on Cool Stars, Stellar Systems, and the Sun, ed. J.-P. Caillault, ASP Conf. Ser., Vol.64, p.174
Mannings V., Emerson J.P. 1994, MNRAS 267, 361
Mayor M., Mermilliod J.-C. 1991, in: Angular Momentum Evolution of Young Stars, eds. S. Catalano, J.R. Stauffer, p.117
Mestel L. 1984, in: 3rd Cambridge Workshop on Cool Stars, Stellar Systems, and the Sun, ed. S.L. Baliunas, L.W. Hartmann, p.49
Meynet G., Mermilliod J.-C., Maeder A. 1993, A&AS 98, 523
Mihalas D. 1973, Stellar Atmospheres, p.536
Neuhaüser R., Sterzik M.F., Schmitt J.H.M.M., Wichmann R., Krautter J. 1995, A&A 297, 391
Noyes R.W., Hartmann L.W., Baliunas S.L., Duncan D.K., Vaughan A.H. 1984, ApJ 279, 763
O'Dell M.A., Panagi P., Hendry M.A., Collier Cameron A. 1995, A&A 294, 715
Osterloh M., Beckwith S.V.W. 1995, ApJ 439, 288
Paatz G., Camenzind M. 1996, A&A 308, 77
Pallavicini R., Golub L., Rosner R., et al. 1981, ApJ 248, 279
Patten B.M., Simon T. 1996, ApJS 106, 489
Pearson K.J., King A.R. 1995, MNRAS 276, 1303
Peterson R.C. 1985, ApJ 294, L35
Pinsonneault M.H., Delyannis C., Demarque P. 1991, ApJ 367, 239
Pinsonneault M.H., Kawaler S.D., Sofia S., Demarque P. 1989, ApJ 338, 424
Pizzo V., Schwenn R., Marsch E., et al. 1983, ApJ 271, 335
Plez B. 1992, A&AS, 94, 527
Popham R. 1996, ApJ 467, 749
Prosser C.F. 1992, AJ 103, 488
Prosser C.F. 1994, AJ 107, 422
Prosser C.F., Grankin K. 1997, in press
Prosser C.F., Randich S., Stauffer J.R., Schmitt J.H.M.M., Simon T. 1996, AJ 112, 1570
Prosser C.F., Stauffer J.R., Caillault J.-P., et al. 1995, AJ 110, 1229

Radick R.R., Thompson D.T., Lockwood G.W., Duncan D.K., Bagget W.E. 1987, ApJ 321, 459
Randich S., Schmitt J.H.M.M., Prosser C.F., Stauffer J.R. 1995, A&A 300, 134
Randich S., Schmitt J.H.M.M., Prosser C.F., Stauffer J.R. 1996, A&A 305, 785
Rogers F.J., Iglesias C.A. 1992, ApJS, 79, 507
Rucínski S.M. 1988, AJ 95, 1895
Ruden S.P., Pollack J.B. 1991, ApJ 375, 740
Saar S.H. 1996, in: MHD Phenomena in the Solar Atmosphere–Prototypes of Stellar Activity, IAU Coll. 153, eds. Y. Uchida, T. Kosugi, H.S. Hudson, in press
Schatzman E. 1962, Annales d'Astrophysique, 25, 18
Schatzman E. 1990, in: Rotation and Mixing in Stellar Interiors, ed. M.-J. Goupil, J.-P. Zahn, Lect. Not. Phys. 366, p.3
Schatzman E. 1993, A&A 279, 431
Schrijver C.J., Pols O.R. 1993, A&A 278, 51; *Erratum:* A&A 293, 640
Shu F., Najita J., Ostriker E., Wilkin F., Ruden S., Lizano S. 1994, ApJ 429, 781
Siess L., Forestini M., Bertout C. 1997, A&A in press
Skrutskie M.K., Dutkevitch D., Strom S.E., et al. 1990a, AJ 99, 1187
Skrutskie M.K., Snell R., Dutkevitch D., et al. 1991, AJ 102, 1749
Skumanich A. 1972, ApJ 171, 565
Soderblom D.R. 1983, ApJS 53, 1
Soderblom D.R. 1996, in: 9th Cambridge Workshop on Cool Stars, Stellar Systems, and the Sun, ed.R. Pallavicini, in press
Soderblom D.R., Mayor M. 1993, ApJ 402, L5
Soderblom D.R., Stauffer J.R., Hudon J.D., Jones B.F. 1993, ApJS 85, 315
Stahler S.W. 1988, ApJ 332, 804
Stauffer J.R., Hartmann L.W. 1987, ApJ 318, 337
Stauffer J.R., Hartmann L.W., Jones B.F. 1989a, ApJ 346, 160
Stauffer J., Hartmann L., Burnham J., Jones B. 1985, ApJ 289, 247
Stauffer J.R., Hartmann L.W., Burton B.F., McNamara B.R. 1989b, ApJ 342, 285
Stauffer J.R., Hartmann L.W., Soderblom D.R., Burnham N. 1984, ApJ 280, 202
Stauffer J.R., Caillault J.-P., Gagné M., Prosser C.F., Hartmann L.W. 1994, ApJS 91, 625
Stauffer J.R., Prosser C.F., Giampapa M.S., Soderblom D.R., Simon T. 1993, AJ 106, 229
Stauffer J.R., Balachandran S.C., Krishnamurthi A., et al. 1997a, ApJ 475, 604
Stauffer J.R., Hartmann L.W., Prosser C.F., et al. 1997b, ApJ, in press
Stepinski T.K., Valageas P. 1996a, A&A 309, 301
Stepinski T.K., Valageas P. 1996b, Lunar & Planetary Science, Vol.27, p.1269
Sterzik M.F., Durisen R.H. 1995, A&A 304, L9
Strom K.M., Strom S.E., Merril K.M. 1993, ApJ 412, 233
Strom K.M., Strom S.E., Edwards S., Cabrit S., Skrutskie M. 1989, AJ 97, 1451
Strom S.E. 1994, in: 8th Cambridge Workshop on Cool Stars, Stellar Systems, and the Sun, ed. J.-P. Caillault, ASP Conf. Ser., Vol.64, p.211
Strom S.E. 1995, Rev.Mex.A&A Conf. Ser., Vol.1, p.317
Strom S.E., Edwards S., Skrutskie M. 1993, in: Protostars & Planets III, ed. E. Levy and J. Lunine (University of Arizona Press), p.837
Tassoul J.-L., Tassoul M. 1989, A&A 213, 397
Tomczyk S., Schou J., Thompson M. 1995, ApJ 448, L57
Tout C.A., Pringle J.E. 1992, MNRAS 259, 604
Trullols E., Jordi C. 1993, A&AS 100, 311
Ulrich R.K. 1993, in: Inside the Stars, IAU Coll.137, eds W.W. Weiss, A. Baglin, ASP Conf. Ser. Vol.40, p.25
Vilhu O. 1984, A&A 133, 117
Walter F.M., Brown A., Mathieu R.D., Myers P.C., Vrba F.J. 1988, AJ 96, 297
Weber E.J., Davis L. 1967, ApJ 148, 217
Wagoner, R.V. 1969, ApJS, 162, 247
Wichmann R., Krautter J., Schmitt J.H.M.M., et al. 1996, A&A 312, 439
Wichmann R., Bouvier J., Allain S., Krautter J. 1997b, A&A submitted
Wichmann R., Krautter J., Covino E., et al. 1997, A&A, in press
Wolk S.J., Walter F.M. 1996, AJ 111, 2066
Zahn J.-P. 1992, A&A 265, 115
Zahn J.-P., Talon S., Matias J. 1997, A&A, in press
Zuckerman B., Becklin E.E. 1993, ApJ 414, 793

This article was processed by the author using Springer-Verlag LaTeX A&A style file *L-AA* version 3.